2023

STEADY STATE AND TRANSIENT ANALYSIS OF HEAT TRANSFER IN A POROUS FIN WITH RADIALLY OUTWARDS PRESSURE-DRIVEN FLOW

Muhammad Mehdi Abbas

STEADY STATE AND TRANSIENT ANALYSIS OF HEAT TRANSFER IN A POROUS FIN WITH RADIALLY OUTWARDS PRESSURE-DRIVEN FLOW

by

MUHAMMAD MEHDI ABBAS

Presented to the Faculty of the Graduate School of

The University of Texas at Arlington in Partial Fulfillment

of the Requirements

for the Degree of

MASTER OF SCIENCE IN MECHANICAL

ENGINEERING

THE UNIVERSITY OF TEXAS AT ARLINGTON

May 2023

Acknowledgements

I would like to express my deepest gratitude to Dr. Jain for his constant support and guidance which made all this possible. I would also like to thank Dhananjay Mishra for guiding and mentoring me. I would like to thank Dr. Mohsen Torabi for his technical help on porous flow and heat transfer. I would like to thank all the members of Microscale Thermophysics laboratory for their encouragement and support throughout my master's research.

I would also like to express sincerest gratitude to my parents and all my family members for believing in me and supporting me throughout my journey.

15th May 2023

Abstract

Thermal management and energy storage problems often utilize extended surfaces, also known as fins for enhanced heat transfer. Today fins are used in a wide range of devices including but not limited to microelectronic components and large heat exchanger. Traditional fins as well as porous fins with flow orthogonal to fin direction have been subject of past research. There is very few academic literature available on porous fins with pressure driven flow along fin direction. While thermal conduction is usually the dominant mode of heat transfer in a solid fin, the use of porous fins that include advective thermal transport due to porous fluid flow has also been investigated. In particular, the steady state and transient thermal performance of a porous fin with pressure-driven radially outwards flow has been studied. It is shown that the transient temperature field in the fin is governed by a convection-diffusion-reaction (CDR) equation, the solution for which is based in the form of Bessel functions. Fin performance is classified for both steady state as well as transient cases with the help of various performance parameters. The steady state case shows that thermal properties of the fin as well as ambient convective conditions strongly impact the relationship between fin porosity and fin performance. While in some cases, it is found that an optimum porosity exists that maximizes heat removal, in other cases, the use of a porous fin is found to be not desirable at all. The analysis presented here helps fully understand these trade-offs and provides useful guidelines for porous fin design for maximum heat removal. Since fin porosity improves advective thermal transport but suppresses diffusive transport at different rates at different times, therefore, it is shown that the impact of fin porosity on heat removal rate depends on the total time over which the fin operates. Consequently, it is important to consider transient effects in determining whether the use of a porous is beneficial at all, and, if so, the

optimal fin porosity. This work contributes towards porous fin theory and offers practical design guidelines for improving and optimizing the performance of porous fins.

TABLE OF FIGURES

TABLE OF CONTENT

CHAPTER 1: INTRODUCTION

Fins play a crucial role in enhancing heat transfer and energy storage in various engineering devices and systems. While conventional fins are typically composed of non-porous materials, recent studies have investigated porous fins with natural convection porous flow perpendicular to the fin direction. However, there is a lack of research on porous fins with fluid flow occurring along the direction of the fin. In such fins, porosity can potentially improve advective heat removal by increasing the flow rate, but it may also hinder conductive heat removal by reducing the effective thermal conductivity. Thus, a comprehensive analysis of the thermal performance of such porous fins is warranted.

This thesis presents a solution for the steady-state and transient temperature distribution in a porous fin with advection along the fin direction. The temperature distribution in such a fin is governed by a convection-diffusion-reaction equation, and a solution is derived in the form of modified Bessel functions of non-zero order. Two distinct parameters are introduced to characterize the performance of porous fins and derived accordingly. The analysis reveals that the thermal properties of the fin and the convective conditions in the surrounding environment strongly influence the relationship between fin porosity and fin performance.

The results demonstrate that, in certain cases, an optimum porosity exists that maximizes heat removal. However, in other scenarios, the use of a porous fin may not be desirable at all. This analysis provides valuable insights into the trade-offs associated with porous fin design and offers practical guidelines for achieving maximum heat removal through porous fins.

By combining the transient thermal analysis of a porous fin with radial porous fluid flow and the steady-state temperature distribution in a porous fin with advection along the fin direction, this work contributes to the understanding of porous fin theory and provides comprehensive design guidelines for improving the transient and steady-state performance of porous fins in thermal management and energy storage applications.

CHAPTER 2: STEADY STATE THERMAL ANALYSIS OF A POROUS FIN WITH RADIALLY OUTWARDS FLUID FLOW

Problem Definition

The problem of interest in this work pertains to heat removal from the outer wall of a hot cylindrical body by a radial fin. The fin is made of a porous material that permits radially outwards fluid flow from the wall towards the tip, as shown schematically in Fig. 1 (a). The lateral surfaces of the fin are assumed to be sealed, so that only radially outwards porous flow is possible. The hot cylindrical body is assumed to be hollow and thin walled, and carrying a fluid within, so that a pressure difference between the inside of the cylindrical body and the tip of the fin results in radially out- wards fluid flow through the fin material.

Heat transfer in the porous fin described above occurs both due to diffusion in the solid and due to advection by fluid flow through the pores of the porous material. This is in contrast with traditional non-porous fins, in which diffusion is the only heat transfer mechanism within the fin. Note that the radial porous fin configuration being analyzed here is distinct from previously studied porous fin configurations, in which, buoyancy-driven fluid flow occurs in a di- rection orthogonal to the fin direction [7, 8, 12 ,13], as opposed to advection-driven flow along the fin in the present work.

The interest here is to derive expressions for the steady state temperature distribution in the porous fin and thus determine its heat transfer performance. Understanding the contributions of diffusion

and advection towards overall heat removal may help identify scenarios where such a porous fin may be particularly effective or ineffective.

The inner and outer radii of the fin are R_0 and, where L is the fin length. The height of the fin is w. Uniform porosity and permeability of the fin material are denoted by φ and κ, respectively. Thermal conductivity, density and heat capacity of the fluid are taken to be k_f, $\rho_f$and c_f, respectively. A similar nomenclature is followed for solid component of the fin, with subscripts.

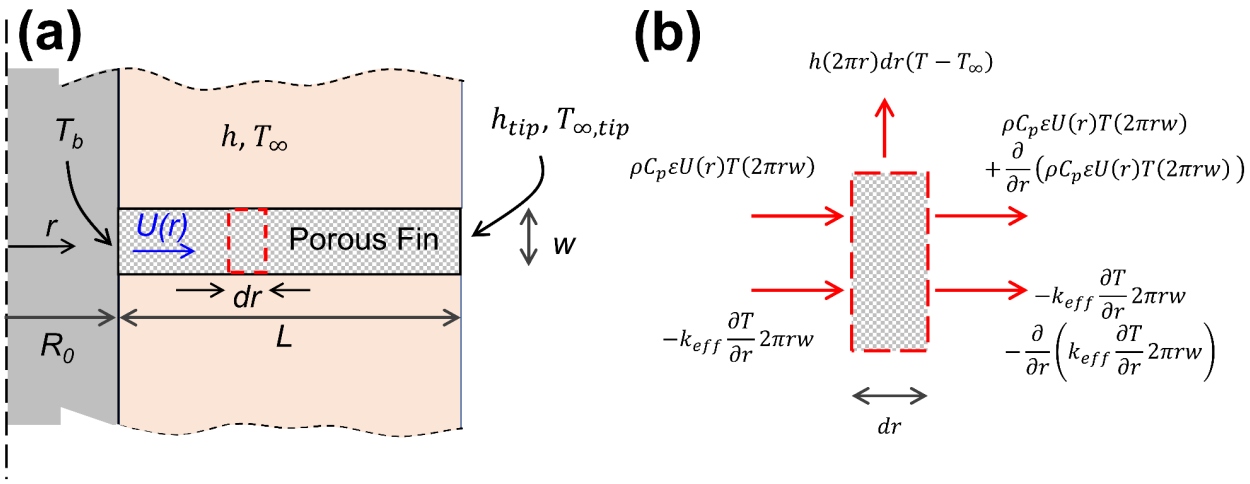

Figure 1.(a) Schematic of the geometry of a porous radial fin with outwards, pressure-driven flow through the pores of the fin material, (b) Schematic of energy balance for an infinitesimal element of the porous fin, showing advective and diffusive transport through the fin as well as convective heat loss to the surrounding medium.

Fluid viscosity is denoted by μ. The effective thermal conductivity of the porous medium is taken to be k_{eff}. The pressure difference between the base ($r = R_0$) and tip ($r = R_0 + L$) of the fin is taken to be Δp. Temperature at the base of the fin is denoted by T_b . Freestream temperature of the medium surrounding the fin is taken to be T_∞. Thermal interactions between the outer surface of the fin and the surrounding ambient are assumed to be represented by a convective heat transfer coefficient h_{tip}. In addition, a convective heat trans- fer coefficient h tip along with an external

freestream temperature T_∞, tip is assumed at the tip of the fin. Note that in many cases, $T_\infty, tip = T_\infty$, although this assumption is not needed/made in this work.

A number of other assumptions are made in order to carry out a thermal analysis of a porous fin. Axisymmetry of the temperature field is assumed. The velocity field is assumed to be only radial, as the fin surfaces are sealed to prevent fluid leakage normal to the fin direction. All transport properties are assumed to be independent of temperature. Radiative heat transfer and natural convection effects around the fin are neglected, due to a reasonably small temperature difference between the fin base and ambient. Note that radiative effects may be modeled approximately by an effective heat transfer coefficient [25], but this is not investigated in de- tail in the present work. The porous flow is assumed to be Newtonian and laminar, and, therefore, governed by the Darcy equation. A constant permeability is assumed. Based on these assumptions, a governing differential equation for the radial temperature distribution in the porous fin may be derived by considering energy conservation in an infinitesimal element at radial location r and of radial dimension dr. As shown in Fig. 1 (b), thermal energy flows in and out of this element include thermal conduction, advection due to radial fluid flow and heat loss/gain from the ambient due to the imposed convective heat transfer coefficient. By carrying out a balance between these energy flow terms in steady state, the following governing energy equation may be derived [1, 2]:

$$\frac{k_{eff}}{r}\frac{\partial}{\partial r}\left(r\frac{\partial T}{\partial r}\right) - \frac{\phi\rho_f c_f}{r}\frac{\partial}{\partial r}(r \cdot T \cdot U(r)) - \frac{h}{w}(T - T_\infty) = 0 \qquad (1)$$

where T(r) and U(r) are the temperature and velocity fields, respectively, within the porous fin. k_{eff} is the effective thermal conductivity of the medium that accounts for thermal conduction

through both solid and fluid constituents. Compared to the standard fin equation [1], Eq. (1) contains an additional term that models advective thermal transport.

Appendix A shows that, based on the Darcy equation for porous flow in radial coordinates, the radial velocity field in the porous fin is given by

$$U(r) = \frac{\mathrm{K} \cdot \Delta p}{\mu \cdot \ln\left(\frac{R_0 + L}{R_0}\right) \cdot r} \tag{2}$$

The 1/r dependence of the velocity field above is consistent with the requirement of mass conservation as the fluid flows radially outwards.

The two boundary conditions associated with Eq. (1) are

$$T = T_b \qquad (r = R_0) \tag{3}$$

$$-k_{eff}\frac{\partial T}{\partial r} = h_{tip}\left(T - T_{\infty,tip}\right) \qquad (r = R_0 + L) \tag{4}$$

The following non-dimensional variables and parameters are introduced:

$$\begin{aligned} \xi = \frac{r}{R_0};\ \theta = \frac{T - T_\infty}{T_b - T_\infty};\ \bar{A} = \frac{\mathrm{K} \cdot \rho_f c_f \cdot \Delta p \cdot \phi}{\mu \cdot \ln\left(\frac{R_0 + L}{R_0}\right) k_{eff}};\ \bar{B} = \frac{hR_0^2}{k_{eff} w};\ \bar{L} = \frac{L}{R_0};\ Bi_{tip} \\ = \frac{h_{tip} R_0}{k_{eff}};\ \theta_{\infty,tip} = \frac{T_{\infty,tip} - T_\infty}{T_b - T_\infty};\ \bar{w} = \frac{w}{R_0} \end{aligned} \tag{5}$$

Note that based on definitions above, $\bar{A}$ may be interpreted as the ratio of advective and diffusive transport, i.e., a Péclet number [10]. Similarly, $\bar{B}$ is the ratio of the term representing heat removal

to the ambient and diffusive thermal transport term [1, 26], similar to the Damköhler number that appears in mass transfer problems [27].

Inserting the form of the velocity field from Appendix A as well as the non-dimensional variables from Eq. (5) into the governing equation given by Eq. (1) results in the following non-dimensional governing energy conservation for the temperature field in the fin

$$\frac{1}{\xi}\frac{\partial}{\partial\xi}\left(\xi\frac{\partial\theta}{\partial\xi}\right)-\frac{\bar{A}}{\xi}\frac{\partial\theta}{\partial\xi}-\bar{B}\theta=0 \tag{6}$$

This is a Convection-Diffusion-Reaction (CDR) equation that ap- pears in several other heat and mass transfer problems including drug delivery [26], reactor engineering [28] and pollution dispersion problems [29]. The non-dimensional boundary conditions as- sociated with this equation are given by

$$\theta=1 \qquad (\xi=1) \tag{7}$$

$$-\frac{\partial\theta}{\partial\xi}=Bi_{tip}\left(\theta-\theta_{\infty,tip}\right) \qquad (\xi=1+\bar{L}) \tag{8}$$

Solution of the Problem

In order to solve Eq. (6), one may substitute $\theta(\xi) = \xi^{\frac{\bar{A}}{2}}\varphi(\xi)$, which can be shown to result in the following equation for φ:

$$\xi^2 \frac{\partial^2 \phi}{\partial \xi^2} + \xi \frac{\partial \phi}{\partial \xi} - \left(\bar{B} \xi^2 + \frac{\bar{A}^2}{4} \right) \phi = 0 \tag{9}$$

which is the modified Bessel equation [30]. Therefore, a solution for the temperature distribution may be written as

$$\theta(\xi) = \xi^{\bar{A}/2} \left[c_1 I_{\bar{A}/2} \left(\sqrt{\bar{B}} \xi \right) + c_2 K_{\bar{A}/2} \left(\sqrt{\bar{B}} \xi \right) \right] \tag{10}$$

where I and K refer to modified Bessel functions of the first and second kind, respectively. $\bar{A}/2$ is the order of the modified Bessel functions. c_1 and c_2 are constants to be determined from the boundary conditions.

Inserting equation (9) into the boundary conditions given by equations (7) and (8) results in the following two linear algebraic equations in c_1 and c_2

$$c_1 I_{\bar{A}/2} \left(\sqrt{\bar{B}} \right) + c_2 K_{\bar{A}/2} \left(\sqrt{\bar{B}} \right) = 1 \tag{10}$$

$$\begin{aligned} \sqrt{\bar{B}}(1+\bar{L})^{\bar{A}/2} \Bigg[& \sqrt{\bar{B}} \left(c_1 I_{\frac{\bar{A}}{2}-1} \left(\sqrt{\bar{B}}(1+\bar{L}) \right) - c_2 K_{\frac{\bar{A}}{2}-1} \left(\sqrt{\bar{B}}(1+\bar{L}) \right) \right) \\ & + Bi_{tip} \left(c_1 I_{\frac{\bar{A}}{2}} \left(\sqrt{\bar{B}}(1+\bar{L}) \right) + c_2 K_{\frac{\bar{A}}{2}} \left(\sqrt{\bar{B}}(1+\bar{L}) \right) \right) \Bigg] \\ & = Bi_{tip} \theta_{\infty,tip} \end{aligned} \tag{11}$$

from where, c_1 and c_2 may be determined as follows

$$c_1 = \frac{-\sqrt{\bar{B}}K_{\frac{\bar{A}}{2}-1}\left(\sqrt{\bar{B}}(1+\bar{L})\right) + Bi_{tip}K_{\frac{\bar{A}}{2}}\left(\sqrt{\bar{B}}(1+\bar{L})\right) - \theta_{\infty,tip}Bi_{tip}(1+\bar{L})^{-\frac{\bar{A}}{2}}K_{\frac{\bar{A}}{2}}\left(\sqrt{\bar{B}}\right)}{-\sqrt{\bar{B}}\left(K_{\frac{\bar{A}}{2}-1}\left(\sqrt{\bar{B}}(1+\bar{L})\right)I_{\frac{\bar{A}}{2}}\left(\sqrt{\bar{B}}\right) + I_{\frac{\bar{A}}{2}-1}\left(\sqrt{\bar{B}}(1+\bar{L})\right)K_{\frac{\bar{A}}{2}}\left(\sqrt{\bar{B}}\right)\right) + Bi_{tip}\left(K_{\frac{\bar{A}}{2}}\left(\sqrt{\bar{B}}(1+\bar{L})\right)I_{\frac{\bar{A}}{2}}\left(\sqrt{\bar{B}}\right) - I_{\frac{\bar{A}}{2}}\left(\sqrt{\bar{B}}(1+\bar{L})\right)K_{\frac{\bar{A}}{2}}\left(\sqrt{\bar{B}}\right)\right)} \quad (12)$$

And

$$c_2 = \frac{\sqrt{\bar{B}}I_{\frac{\bar{A}}{2}-1}\left(\sqrt{\bar{B}}(1+\bar{L})\right) + Bi_{tip}I_{\frac{\bar{A}}{2}}\left(\sqrt{\bar{B}}(1+\bar{L})\right) - \theta_{\infty,tip}Bi_{tip}(1+\bar{L})^{-\frac{\bar{A}}{2}}I_{\frac{\bar{A}}{2}}\left(\sqrt{\bar{B}}\right)}{\sqrt{\bar{B}}\left(I_{\frac{\bar{A}}{2}-1}\left(\sqrt{\bar{B}}(1+\bar{L})\right)K_{\frac{\bar{A}}{2}}\left(\sqrt{\bar{B}}\right) + K_{\frac{\bar{A}}{2}-1}\left(\sqrt{\bar{B}}(1+\bar{L})\right)I_{\frac{\bar{A}}{2}}\left(\sqrt{\bar{B}}\right)\right) + Bi_{tip}\left(I_{\frac{\bar{A}}{2}}\left(\sqrt{\bar{B}}(1+\bar{L})\right)K_{\frac{\bar{A}}{2}}\left(\sqrt{\bar{B}}\right) - K_{\frac{\bar{A}}{2}}\left(\sqrt{\bar{B}}(1+\bar{L})\right)I_{\frac{\bar{A}}{2}}\left(\sqrt{\bar{B}}\right)\right)} \quad (13)$$

This completes the solution for the fin temperature field.

Note that the effective thermal conductivity k_{eff} appearing in equation (1) combines thermal conduction in both solid and fluid constituents of the porous fin. In general, k_{eff} depends on the porosity of the medium. While a number of theoretical models are available to compute k_{eff}, in the present work, it is computed simply as the weighted average of thermal conductivities of the solid and fluid constituents, i.e.,

$$k_{eff} = (1 - \phi)k_s + \phi k_f \tag{10}$$

where k_s and k_f are the thermal conductivities of the solid and fluid, respectively.

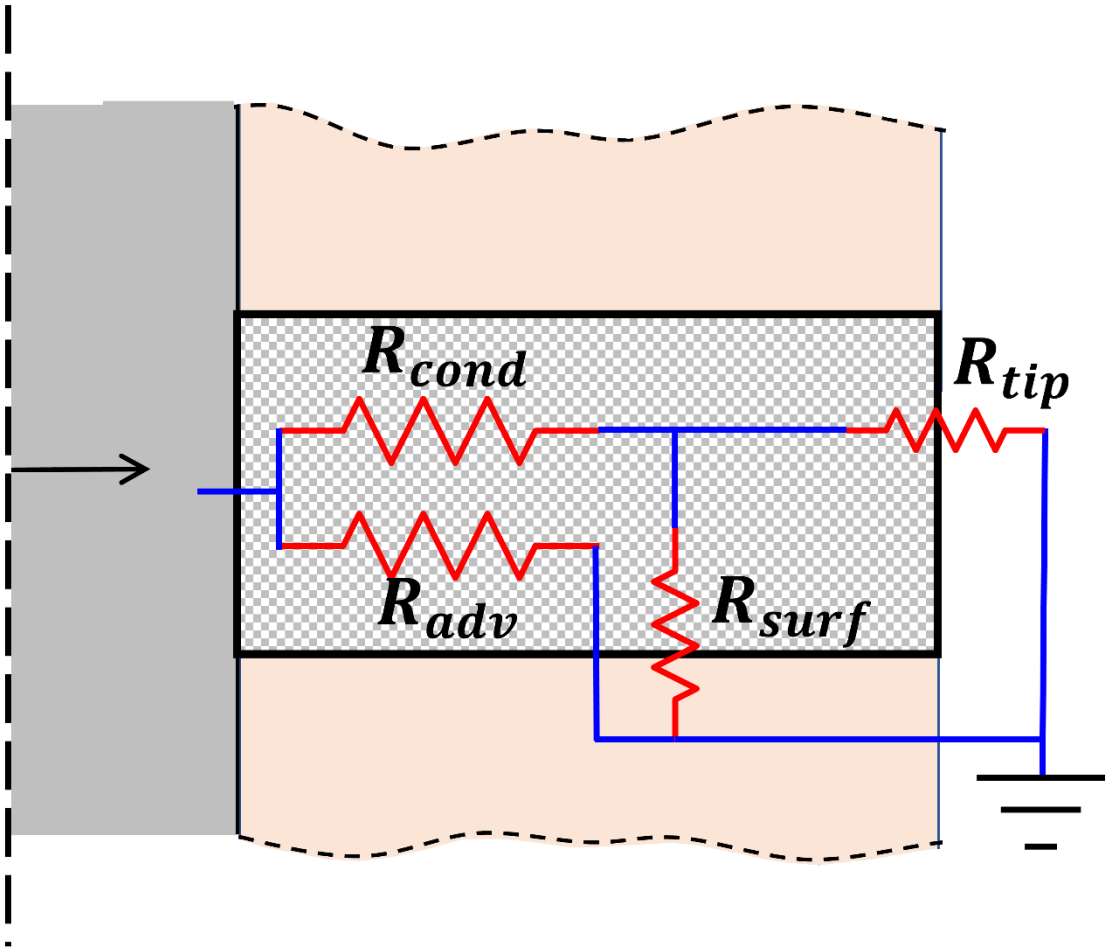

Figure 2. An approximate schematic of the thermal resistance network of the porous fin showing conductive and advective heat removal from the base, followed by dissipation into the ambient through the fin surface and fin tip.

In order to help understand the relative role of advective and conductive heat removal mechanisms, as well as the influence of various problem parameters, heat transfer in this problem may be represented approximately by a thermal resistance network of the porous fin shown in Fig. 2. Heat from the base is removed by the fin through conduction and advection, which are distinct mechanisms that operate in parallel as represented by the resistances R cond and R adv in conductive and advective heat removal from the base, as well as dissipation into the ambient through the fin surface and fin tip.

Fin Performance Parameters

A number of performance parameters are commonly used to compare the rate of heat removal by the fin with idealized and baseline cases [1]. In the present porous fin analysis, two specific cases are of interest. Firstly, performance of the porous fin may be compared with a baseline case with no fin at all, in which case, heat removal occurs purely due to convective heat transfer directly from the base of the fin into the ambient. Another interesting comparison is between heat removal by the porous fin with a comparable non-porous fin. This may help understand the impact of porosity of the fin material and subsequent pressure-driven flow on heat removal.

In order to carry out such comparisons, the heat removal rate from the porous fin must be determined first. Heat is removed from the base of the fin due to both diffusion and advection. Thus, the heat removal rate may be written as

$$q = \left(-k_{eff} \left(\frac{\partial T}{\partial r} \right)_{r=R_0} + \phi \rho_f c_f \cdot \mathrm{U}(R_0)(T_b - T_\infty) \right) 2\pi R_0 w \tag{16}$$

Thus, a non-dimensional heat removal rate may be defined as follows

$$\begin{aligned} \bar{q} = \frac{q}{k_{eff}(T_b - T_\infty)2\pi w} &= -\left(\frac{\partial \theta}{\partial \xi} \right)_{\xi=1} + \bar{A} \\ &= -\sqrt{\bar{B}} \left(c_1 I_{\frac{\bar{A}}{2}-1}\left(\sqrt{\bar{B}}\right) - c_2 K_{\frac{\bar{A}}{2}-1}\left(\sqrt{\bar{B}}\right) \right) + \bar{A} \end{aligned} \tag{17}$$

where the first and second terms represent conductive and advective heat transfer rates, respectively.

Comparison with no fin case

The ratio of heat removed by the fin and heat removed without the fin is usually referred to as the fin effectiveness [1]. In the present case, the rate of heat removed without the fin is simply $h(T_b - T_\infty)2\pi R_0 w$. Using this in conjunction with Equation (16), the following expression for fin effectiveness may be obtained

$$\eta = \frac{1}{\overline{w}\overline{B}}\left(-\left(\frac{\partial\theta}{\partial\xi}\right)_{\xi=1} + \bar{A}\right) = \frac{1}{\overline{w}\overline{B}}\left(\bar{A} - \sqrt{\overline{B}}\left(c_1 I_{\frac{\bar{A}}{2}-1}\left(\sqrt{\overline{B}}\right) - c_2 K_{\frac{\bar{A}}{2}-1}\left(\sqrt{\overline{B}}\right)\right)\right) \tag{18}$$

For a well-designed fin, η must be larger than one, since the fin is expected to remove more heat than would be removed without it.

4.2. Comparison with non-porous fin case

In order to quantify the benefit of porous flow in the fin, one may define a porous fin effectiveness, η_{porous} by comparing the heat removed by the porous fin with heat removed by a comparable non-porous fin of the same dimensions and in the same conditions. η_{porous} quantifies whether it is beneficial to replace a solid fin with a porous fin under the same operating conditions. On one hand, compared to the non-porous fin, the porous fin offers greater heat removal due to advection along with the radially outwards porous fluid flow. However, it may also suffer from reduced heat removal by conduction down the fin due to the expected reduction in effective thermal conductivity of the fin compared to that of the baseline non-porous fin.

In order to understand which of these effects may dominate, one may compute the heat removed by a non-porous fin using the results presented here, but with $\bar{A} = 0$ and using thermal conductivity of the solid material instead of the effective thermal conductivity. By doing so, the following expression for the porous fin effectiveness may be derived.

$$\eta_{porous} = \frac{k_{eff}}{k_s} \frac{\bar{A} - \sqrt{\bar{B}}\left(c_1 I_{\frac{\bar{A}}{2}-1}\left(\sqrt{\bar{B}}\right) - c_2 K_{\frac{\bar{A}}{2}-1}\left(\sqrt{\bar{B}}\right)\right)}{-\sqrt{\overline{B_s}}\left(c_{1,s} I_1\left(\sqrt{\overline{B_s}}\right) - c_{2,s} K_1\left(\sqrt{\overline{B_s}}\right)\right)} \tag{19}$$

where $\bar{B}_s = \frac{hR_0^2}{k_s w}$ and k_s refers to thermal conductivity of the solid material. The coefficients $c_{1,s}$ and $c_{2,s}$ are obtained from the boundary conditions corresponding to the zero-advection non-porous fin problem, i.e., by setting $\bar{A} = 0$ and $\bar{B} = \bar{B}_s$ in Equations (13) and (14).

η and η_{porous} defined above are important fin performance metrics that characterize how well the porous fin performs compared to cases without a fin at all and with a comparable but non-porous fin. While η represents how well the porous fin performs compared to no fin at all, η_{porous} governs whether the porous fin is better than an equivalent non-porous fin. These parameters also help understand the impact of various problem parameters, such as porosity on fin performance.

Special Cases

Special cases for transport conditions

The general problem solved in Section 2 accounts for both conduction and advection driven heat transfer down the fin. While both mechanisms may be important in general, two special cases in which one or the other mechanism dominates may be of interest in specific applications.

Negligible diffusion

In certain cases, diffusion may be negligible compared to advection, for example when the flow velocity is relatively large. In order to model this special case, the first term on the left hand of the governing equation, given by Equation (6) may be neglected. This results in the following simplified governing equation

$$\frac{\bar{A}}{\xi}\frac{\partial\theta}{\partial\xi} + \bar{B}\theta = 0 \tag{20}$$

As expected, in the absence of diffusion, the governing equation becomes a first-order differential equation, for which, only the upstream boundary condition ($\theta = 1$ at $\xi = 0$) is needed. The solution for the temperature distribution in the fin is given by

$$\theta(\xi) = \exp\left(-\frac{\bar{B}}{\bar{A}}\xi^2\right) \tag{21}$$

which is indeed the solution for a pure-advection problem [26].

Note that $\bar{B}/\bar{A} = \frac{hR_0^2 \cdot \mu \cdot \ln\left(\frac{R_0+L}{R_0}\right)}{\mathrm{K} \cdot \rho_f c_f \cdot \Delta p \cdot \phi \cdot w}$, i.e., thermal conductivity of the fin does not appear in the expression for the temperature distribution. This is to be expected since diffusion is assumed to be negligible in this special case.

Negligible advection

The other extreme scenario of potential interest is where advection is small or negligible. In such a case, the second term on the left hand of the governing energy equation may be neglected. This results in

$$\frac{1}{\xi}\frac{\partial}{\partial \xi}\left(\xi \frac{\partial \theta}{\partial \xi}\right) - \bar{B}\theta = 0 \tag{22}$$

which is indeed the standard governing equation for a purely diffusive fin. A general solution for this problem obtained by setting $\bar{A} = 0$ in the general solution, Equation (10) is

$$\theta(\xi) = \left[c_1 I_0\left(\sqrt{\bar{B}}\xi\right) + c_2 K_0\left(\sqrt{\bar{B}}\xi\right)\right] \tag{23}$$

which matches with the standard solution for this pure-diffusive problem [1].. The constants appearing in Equation (23) may be obtained using boundary conditions, similar to the general case considered in Section 2. For example, for an adiabatic tip, one may derive

$$\theta(\xi) = \frac{K_1\left(\sqrt{\bar{B}}(1+\bar{L})\right) I_0\left(\sqrt{\bar{B}}\xi\right) + I_1\left(\sqrt{\bar{B}}(1+\bar{L})\right) K_0\left(\sqrt{\bar{B}}\xi\right)}{K_1\left(\sqrt{\bar{B}}(1+\bar{L})\right) I_0\left(\sqrt{\bar{B}}\right) + I_1\left(\sqrt{\bar{B}}(1+\bar{L})\right) K_0\left(\sqrt{\bar{B}}\right)} \tag{24}$$

Tip boundary special cases

While the model presented in Section 2 assumes general convective boundary conditions at the tip, including a general tip ambient temperature, depending on the specific conditions encountered in a problem, a number of simplifications may be considered.

A commonly encountered special case is that of an adiabatic tip. This may be relevant, for example, when heat transfer at the tip may be negligible due to the small tip area, or because the fin is very long. In either case, temperature distribution in the fin may be obtained by setting $Bi_{tip} = 0$ in Equations (10), (13) and (14), resulting in

$$\theta(\xi) = \xi^{\bar{A}/2} \frac{K_{\frac{\bar{A}}{2}-1}\left(\sqrt{\bar{B}}(1+\bar{L})\right) I_{\bar{A}/2}\left(\sqrt{\bar{B}}\xi\right) + I_{\frac{\bar{A}}{2}-1}\left(\sqrt{\bar{B}}(1+\bar{L})\right) K_{\bar{A}/2}\left(\sqrt{\bar{B}}\xi\right)}{K_{\frac{\bar{A}}{2}-1}\left(\sqrt{\bar{B}}(1+\bar{L})\right) I_{\frac{\bar{A}}{2}}\left(\sqrt{\bar{B}}\right) + I_{\frac{\bar{A}}{2}-1}\left(\sqrt{\bar{B}}(1+\bar{L})\right) K_{\frac{\bar{A}}{2}}\left(\sqrt{\bar{B}}\right)} \tag{25}$$

While the adiabatic tip excludes any heat transfer at the tip, the opposite, best-case scenario for heat transfer at the tip arises when the tip is specified to be at a certain temperature $\theta_{\infty,tip}$. Results for this case may be obtained by setting $Bi_{tip} \to \infty$ in Equations (10), (13) and (14), which results in

$$\theta(\xi) = \xi^{\bar{A}/2} \frac{\left(K_{\frac{\bar{A}}{2}}\left(\sqrt{\bar{B}}(1+\bar{L})\right) - \theta_{\infty,tip} K_{\frac{\bar{A}}{2}}\left(\sqrt{\bar{B}}\right)\right) I_{\bar{A}/2}\left(\sqrt{\bar{B}}\xi\right) - \left(I_{\frac{\bar{A}}{2}}\left(\sqrt{\bar{B}}(1+\bar{L})\right) - \theta_{\infty,tip} I_{\frac{\bar{A}}{2}}\left(\sqrt{\bar{B}}\right)\right) I_{\bar{A}/2}\left(\sqrt{\bar{B}}\xi\right)}{K_{\frac{\bar{A}}{2}}\left(\sqrt{\bar{B}}(1+\bar{L})\right) I_{\frac{\bar{A}}{2}}\left(\sqrt{\bar{B}}\right) - I_{\frac{\bar{A}}{2}}\left(\sqrt{\bar{B}}(1+\bar{L})\right) K_{\frac{\bar{A}}{2}}\left(\sqrt{\bar{B}}\right)} \tag{26}$$

Finally, in many scenarios, the freestream temperature associated with the convective boundary condition at the tip is the same as the ambient temperature, i.e., $\theta_{\infty,tip} = 0$. In such a case, temperature distribution in the fin further simplifies to

$$\theta(\xi) = \xi^{\bar{A}/2} \frac{K_{\frac{\bar{A}}{2}}\left(\sqrt{\bar{B}}(1+\bar{L})\right) I_{\bar{A}/2}\left(\sqrt{\bar{B}}\xi\right) - I_{\frac{\bar{A}}{2}}\left(\sqrt{\bar{B}}(1+\bar{L})\right) I_{\bar{A}/2}\left(\sqrt{\bar{B}}\xi\right)}{K_{\frac{\bar{A}}{2}}\left(\sqrt{\bar{B}}(1+\bar{L})\right) I_{\frac{\bar{A}}{2}}\left(\sqrt{\bar{B}}\right) - I_{\frac{\bar{A}}{2}}\left(\sqrt{\bar{B}}(1+\bar{L})\right) K_{\frac{\bar{A}}{2}}\left(\sqrt{\bar{B}}\right)} \tag{27}$$

Expressions for fin performance parameters, including heat removal rate, fin effectiveness and porous fin effectiveness can be simplified similarly.

Results and Discussion

Impact of $\bar{A}$ and $\bar{B}$ on fin temperature distribution

$\bar{A}$ and $\bar{B}$ are the two key non-dimensional parameters that appear in the governing energy equation, and consequently in the expressions for temperature distribution and fin performance parameters. $\bar{A}$ represents heat advection due to the radial porous flow in the fin driven by the imposed pressure gradient, relative to diffusive heat flow, and thus, is a Péclet number. On the other hand, $\bar{B}$ represents the rate of heat loss from the fin surface to the surrounding, also relative to diffusive heat flow, and is similar to the Damköhler number in mass transfer analysis. It is pertinent to

examine the impact of these key non-dimensional parameters on the fin temperature distribution and fin performance.

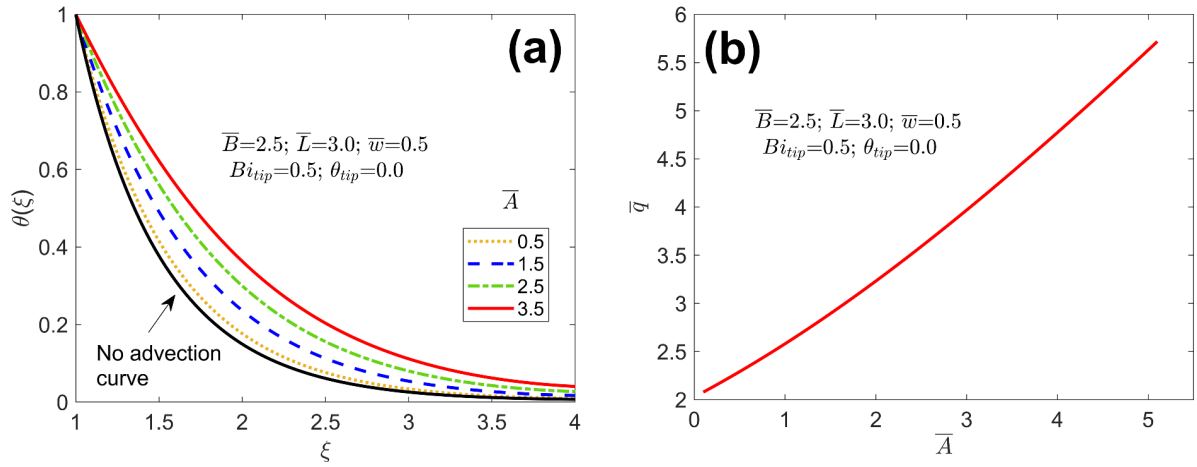

Figure 3. Impact of $\bar{A}$: (a) fin temperature distribution for multiple values of $\bar{A}$, (b) heat transfer rate $\bar{q}$ as a function of $\bar{A}$.

Figure 3 examines the impact of $\bar{A}$. A number of temperature distribution curves for different values of $\bar{A}$ are plotted in Figure 3(a). The values of other parameters are $\bar{B} = 2.5$, $\bar{L} = 3.0$, $\overline{w} = 0.5$, $Bi_{tip} = 0.5$ and $\theta_{\infty,tip} = 0.0$. For comparison, the zero advection curve corresponding to a non-porous fin is also plotted. Figure 3(a) shows that the fin temperature curves shift upwards with increasing value of $\bar{A}$, which can be attributed to greater heat removal down the fin at large $\bar{A}$ due to advection, which increases the fin temperature in general. The curves for various values of $\bar{A}$ approach the limiting case of the traditional non-porous fin as $\bar{A}$ decreases. Note that in each case, as expected, the temperature at the fin base ($\xi = 1$) has a value of 1, whereas the magnitude and gradient of the temperature distribution at the fin tip, $\xi = 1 + \bar{L}$, is determined by the convective boundary condition at the tip.

The impact of $\bar{A}$ on fin performance is further shown in Figure 3(b), in which the total heat removed by the fin, Equation (17), is plotted as a function of $\bar{A}$. Even though conductive heat removal decreases with increasing $\bar{A}$, as evidenced by the decreasing slope of temperature plots at the base seen in Figure 3(a), yet, the increased advective heat transfer at large $\bar{A}$ results in increasing total heat removed with increasing $\bar{A}$.

Note that several dimensional parameters and properties contribute towards $\bar{A}$, as defined in Equation (5). For example, increasing the permeability or pressure gradient, reducing the viscosity or reducing the fin length relative to its radius all contribute towards increasing $\bar{A}$, and thus improving fin performance. Note that the fin porosity impacts fin performance in a more complicated manner, because while $\bar{A}$ increases with increasing fin porosity, it also reduces the effective thermal conductivity k_{eff}, thereby affecting other non-dimensional parameters such as $\bar{B}$ too. This is examined in more detail in a later sub-section.

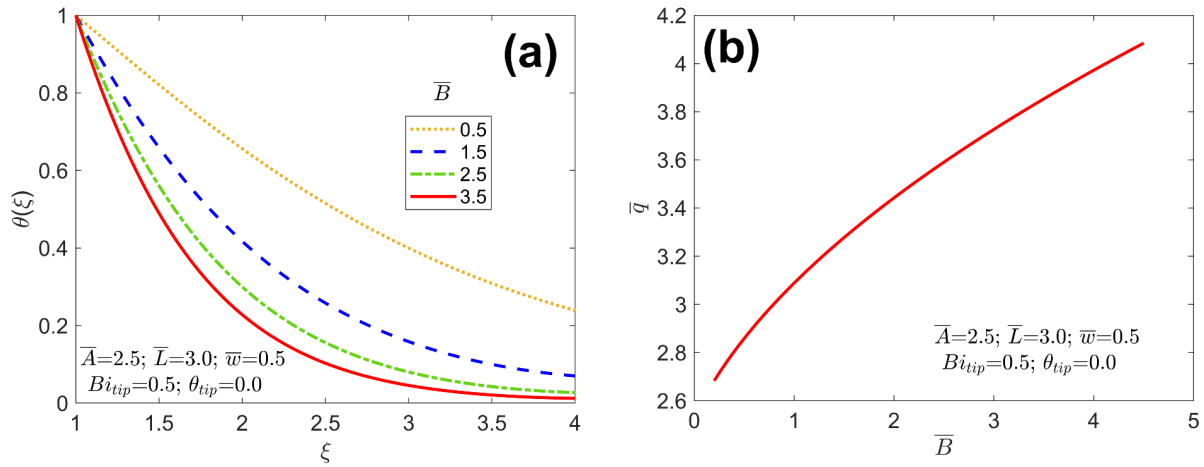

Figure 4. Impact of $\bar{B}$: (a) fin temperature distribution for multiple values of $\bar{B}$, (b) heat transfer rate $\bar{q}$ as a function of $\bar{B}$.

In contrast with $\bar{A}$, which represents advective cooling, $\bar{B}$ represents heat removal due to convective heat transfer from the fin surface to the surrounding ambient. The impact of $\bar{B}$ on fin temperature distribution and heat removal is investigated in Figure 4. Fin temperature curves for multiple values of $\bar{B}$ are plotted in Figure 4(a), whereas total heat removal is plotted as a function of $\bar{B}$ in Figure 4(b). All other problem parameters are the same as Figure 3, along with $\bar{A} = 2.5$. As expected, the larger the value of $\bar{B}$, the greater is the heat removed from the fin, and, therefore, the cooler is the fin. Figure 4(a) also shows strong dependence of the slope of the temperature curve at the fin base on $\bar{B}$, which indicates greater heat removal from the base as $\bar{B}$ increases. This is also seen more directly in the heat removal plot in Figure 4(b), where the heat removed by the fin is seen to increase with increasing value of $\bar{B}$.

Per Equation (5), the key physical quantity that appears in the expression for $\bar{B}$ is the convective heat transfer coefficient around the fin, h. All other parameters being the same, the greater the value of h, the greater is the heat removal to surroundings, and therefore, the more effective is the fin. This is clearly seen in Figures 4(a) and 4(b). Note that while several other dimensional parameters also appear in the expression for $\bar{B}$, most notably the effective thermal conductivity (as well as the porosity that appears within k_{eff}), these parameters also influence other non-dimensional numbers. Therefore, the influence of these parameters is analyzed separately in a later section.

Fin Performance Parameters

Section 4 defines two key performance parameters of the fin. These parameters represent how much heat is removed by the porous fin relative to the no fin case, and relative to a comparable non-porous fin. The impact of key non-dimensional numbers appearing in the problem – $\bar{A}$ and $\bar{B}$ – on these two parameters is investigated in detail.

Fin Effectiveness, η

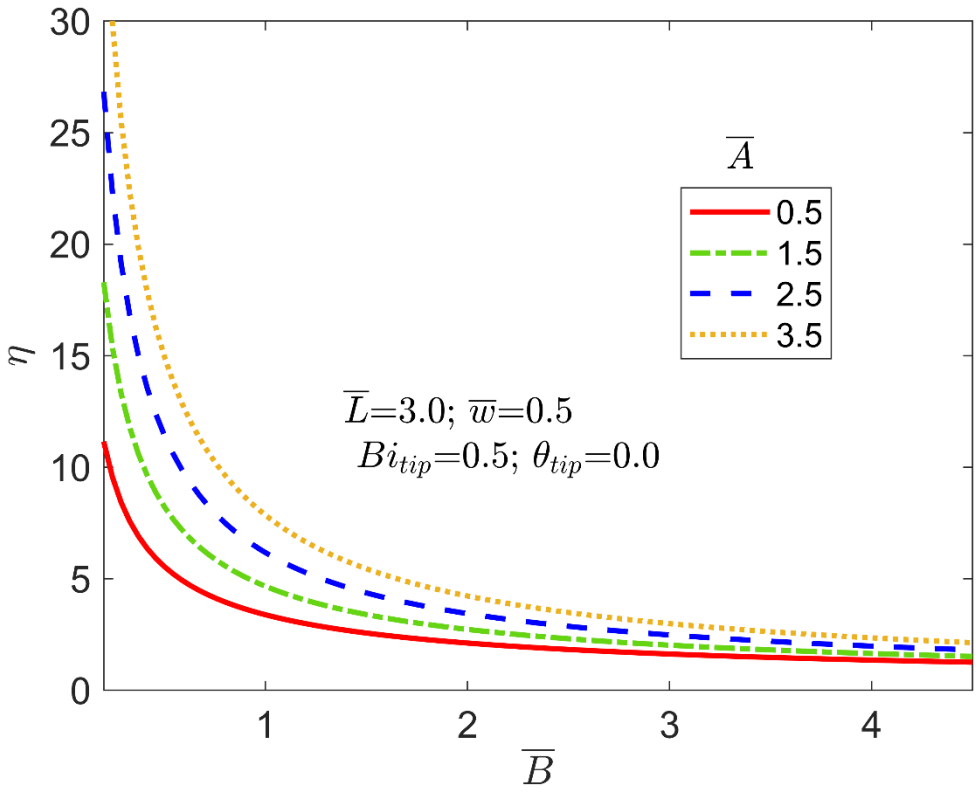

Figure 5. Fin effectiveness as a function of $\bar{B}$ for multiple values of $\bar{A}$.

The fin effectiveness, η is considered first. As defined in Equation (18), η represents heat removal by the porous fin relative to the baseline case without any fin at all. Figure 5 plots η as the function

of the non-dimensional convective heat transfer coefficient $\bar{B}$. Curves are presented for multiple values of $\bar{A}$. In each case, fin effectiveness reduces with increasing $\bar{B}$, rapidly at first, followed by a plateau at larger values of $\bar{B}$. Also, the curves in Figure 5 shift upwards with increasing value of $\bar{A}$. This is because the larger than value of $\bar{B}$, the greater is the amount of conductive heat removed from the fin. In contrast, $\bar{A}$ simply appears as an additional term in the fin effectiveness expression given in Equation (18), and, therefore simply shifts the curves upwards.

The impact of $\bar{B}$ is also confirmed from Figure 4(a) that shows increasing magnitude of the slope of the temperature curve at $\xi = 1$ at increasing value of $\bar{B}$. Since convective heat removal is not influenced by $\bar{B}$, this explains the trend in the curves in Figure 5. Further, Figure 4(a) shows that the slope of the temperature curve does not change at larger values as rapidly as at smaller values, which explains the plateauing out of the curves in Figure 5.

These results indicate that when the non-dimensional convective heat transfer coefficient is relatively large, increasing the advective heat removal, for example, by making the fin more porous does not significantly improve fin performance. This is because the rate-limiting step is the conductive heat removal from the fin. The impact of porosity on performance of the porous fin is likely to be significant when the convective heat removal from the fin surface is not very strong, for example, in conditions approaching natural convection around the fin.

The fin effectiveness plotted in Figure 5 is found to be greater than one throughout the parameter space considered here, indicating that more heat is removed by the fin than without, which is desirable. It is found that the fin effectiveness flattens out at large values of $\bar{B}$. This is because

when the convective heat transfer coefficient around the fin is very large, then the effect of increased surface area of the fin is not very significant any more.

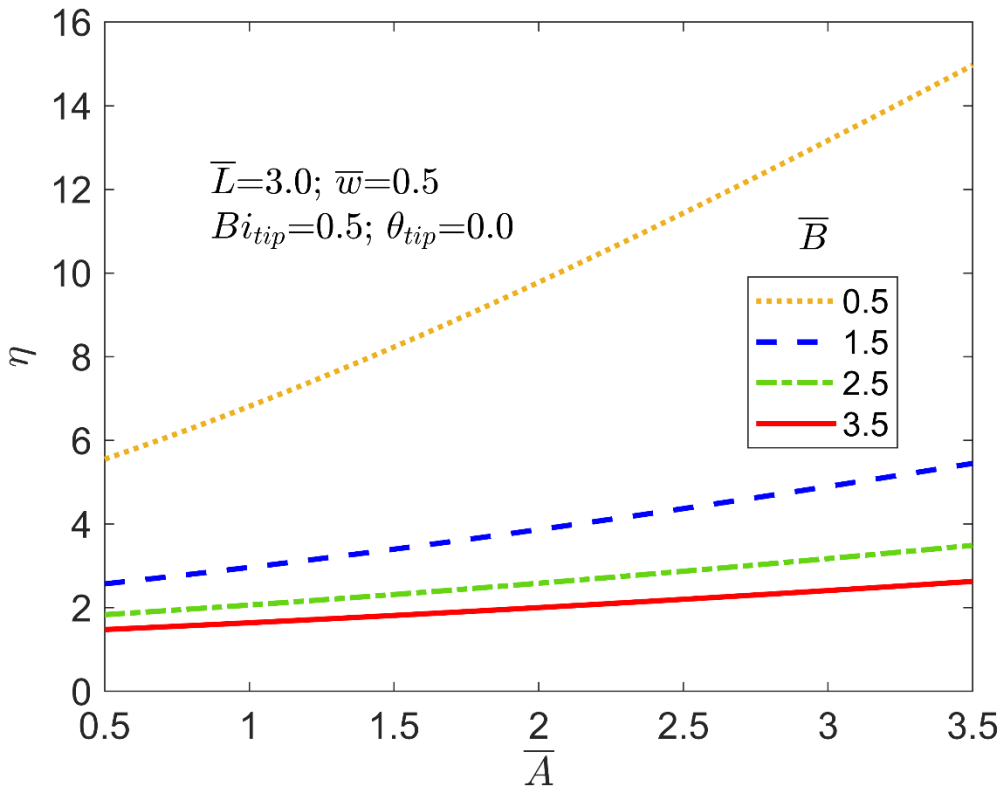

Figure 6. Fin effectiveness as a function of $\bar{A}$ for multiple values of $\bar{B}$.

In contrast with Figure 5, fin effectiveness is plotted as a function of $\bar{A}$ in Figure 6. As expected, fin effectiveness increases monotonically with $\bar{A}$, which is because $\bar{A}$ appears as an independent term in the expression of η, given by Equation (18). As expected, the larger the value of $\bar{B}$, the lower are the effectiveness curves in Figure 6. This is mainly because, as shown and discussed in Figure 5, fin effectiveness reduces with increasing $\bar{B}$.

Porous Fin Effectiveness, η_{porous}

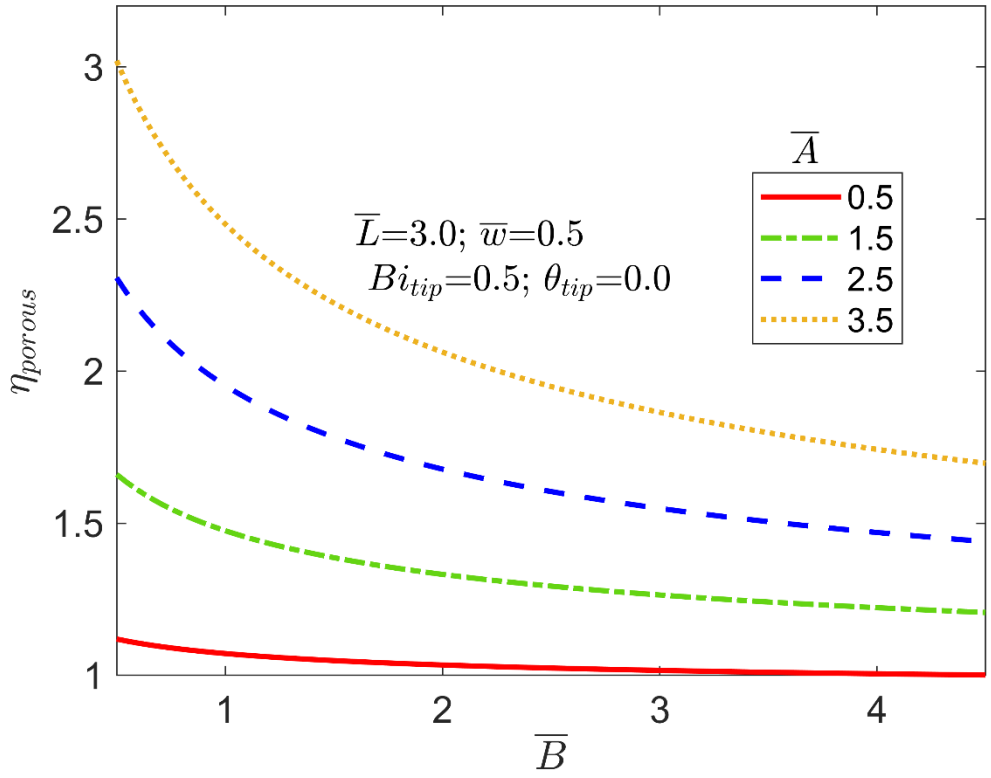

Figure 7. Porous fin effectiveness as a function of $\bar{B}$ for multiple values of $\bar{A}$.

The porous fin effectiveness, η_{porous} which compares performance of the porous fin with that of a comparable non-porous fin is considered next. Similar to Figures in the previous sub-section, η_{porous} is plotted as a function of $\bar{B}$ for multiple values of $\bar{A}$ in Figure 7, and as a function of $\bar{A}$ for multiple values of $\bar{B}$ in Figure 8. These curves show strong dependence of η_{porous} on $\bar{A}$, and relatively weaker dependence on $\bar{B}$, particularly at small $\bar{A}$. This is mainly because the key difference between the porous fin and the non-porous fin is the porous convective term $\bar{A}$. The greater the value of $\bar{A}$, the greater is the heat removal by the porous fin compared to the non-porous fin, which is completely unaffected by $\bar{A}$. This can also be confirmed mathematically from

the expression of $\bar{q}$, given by Equation (17). Therefore, the porous fin becomes more and more attractive compared to the non-porous fin as $\bar{A}$ increases.

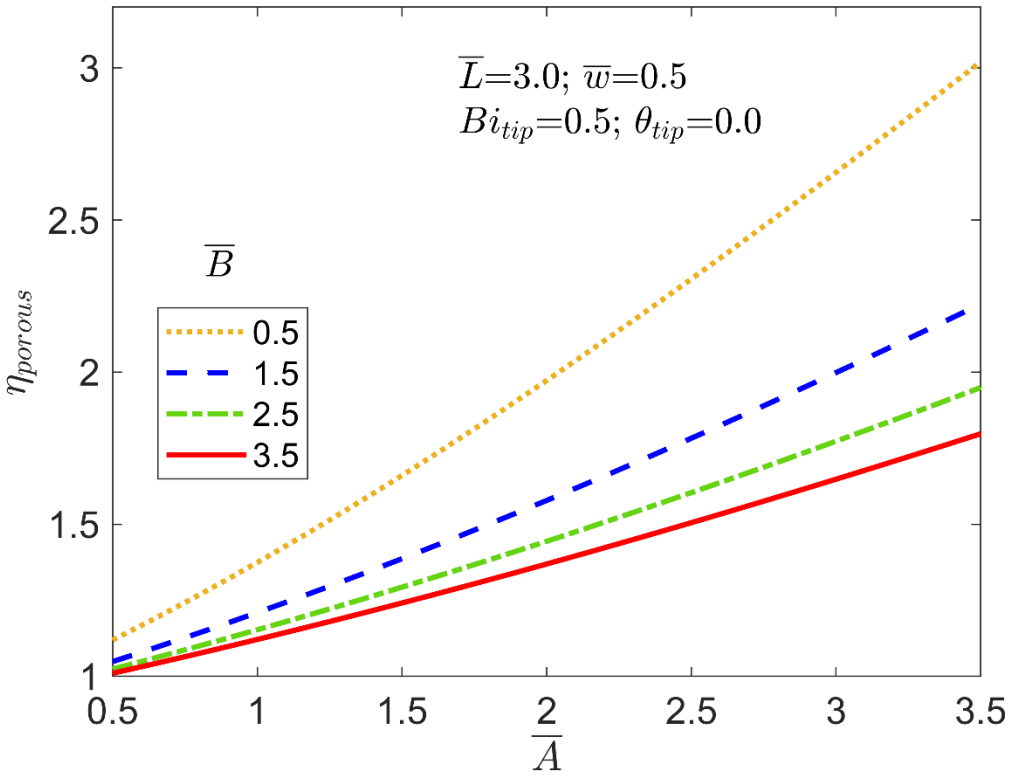

Figure 8. Porous fin effectiveness as a function of $\bar{A}$ for multiple values of $\bar{B}$.

In contrast, the porous fin effectiveness is largely independent of $\bar{B}$, particularly for small values of $\bar{A}$. This is because when $\bar{A}$ is small, there is no particular distinction between the porous and non-porous fin, and no particular thermal advantage of the porous fin over the non-porous fin. Since $\bar{B}$ is expected to affect both porous and non-porous fins similarly, therefore, when $\bar{A}$ is small, the fin performance is not significantly impacted by $\bar{B}$, and η_{porous} is close to one, indicating that the porous and non-porous fins have nearly the same performance.

Effect of porosity: Trade-off between conductive and advective heat removal

The parallel placement of R_{cond} and R_{adv} in the resistance network shown in Figure 2 presents interesting trade-offs and opportunities for optimization of fin performance. Specifically, it is of interest to examine how these two components change as the porosity of the fin is changed since changing the porosity of the fin material is an important design question. In general, increasing the porosity is expected to reduce the effective thermal conductivity, per Equation (15), since the solid material comprising the fin is likely to have greater thermal conductivity than the fluid. This is expected to lead to reduced conductive heat removed by the fin. On the other hand, greater porosity also results in greater area available for porous fluid flow, and, thus, greater advective heat removal. Mathematically, this can be seen in the $\bar{A}$ term that increases with increasing porosity due to the ϕ and k_{eff} terms in the numerator and denominator, respectively, and that results in greater fin heat removal, per Equation (5). Moreover, the porosity ϕ appearing in the advection term in the energy conservation equation given by Equation (1) also shows the enhancement in advective heat removal due to increased porosity. The opposing effects of porosity on conductive and advective heat removal pose an interesting theoretical question about whether an optimal porosity exists that maximizes or minimizes total heat removal. This is also a question of much practical relevance, and, therefore, is investigated in more detail.

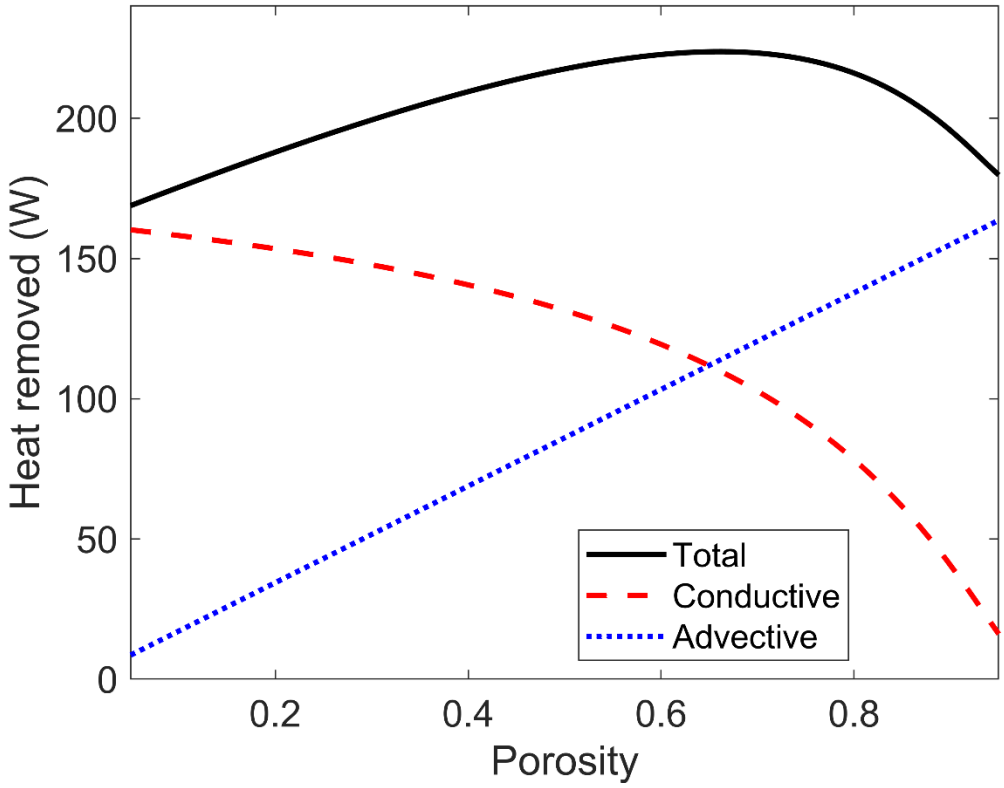

Figure 9. Heat removal rate as a function of fin porosity for a baseline set of design parameters. Total heat removed as well as the conductive and advective components are plotted.

To begin with, heat removed by a representative porous fin is considered. The baseline solid material is assumed to be aluminum, and the fluid is assumed to be air, with constant properties corresponding to room temperature. Permeability of the fin is taken to be $K=5.7\times10^{-9}$ m^2. The inner radius fin length and fin width are taken to be R_0=5 cm, L=15 cm and w=5 cm, respectively. The pressure difference driving the porous flow is taken to be Δp=100 Pa. The convective heat transfer coefficient, both around the fin and at the tip is taken to be h=50 Wm^{-2}K^{-1}. Under these conditions, Figure 9 presents the total heat removed as well as the conductive and advective components as functions of porosity, corresponding to 20 °C temperature difference between the base and ambient. As expected from the discussion above, the conductive and advective

components of heat removed decrease and increase, respectively, with increasing porosity. While the advective component increases nearly linearly, the advective component has a more complicated, non-linear reduction. This is because porosity increases the advective term in the governing energy equation ($\bar{A}$) linearly, whereas the impact of porosity on conductive heat transfer is more complicated, driven by the slope of the temperature distribution at the base, as given by the solution involving modified Bessel functions. Interestingly, in this case, the total heat removed changes non-monotonically with porosity and exhibits a maxima at a porosity of around 0.65. This shows the importance of careful design of the porous fin, particularly its porosity in order to maximize the effectiveness of the fin and the benefit of the porous flow.

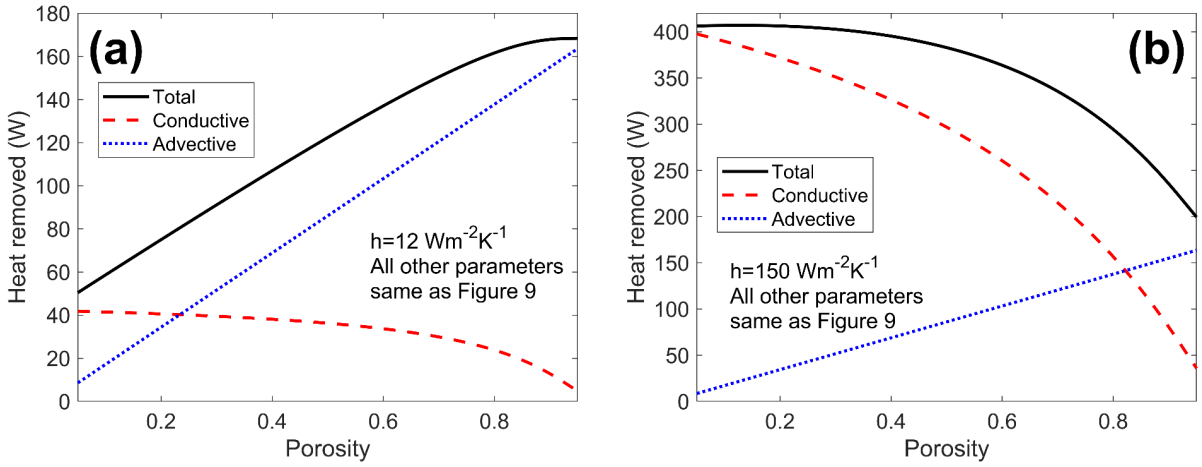

Figure 10. Heat removal rate as a function of fin porosity for (a) h=10 $W.m^{-2}.K^{-1}$ and (b) h=150 $W.m^{-2}.K^{-1}$. Other parameters are the same as Figure 9. Total heat removed as well as the conductive and advective components are plotted.

Note that the impact of porosity of fin effectiveness is highly complicated due to the number of ways in the porosity affects heat removal rate, depending on the values of various problem parameters and non-dimensional numbers that appear in the analysis presented above. While an optimal porosity is found for the set of parameters considered above, the location of the optimal

porosity, or even the existence of an optimal porosity itself is not universal. For example, the impact of the convective heat transfer on these curves is examined. Figures 10(a) and 10(b) plot the total heat removed as well as the conductive and advective components as functions of porosity for h=12 $Wm^{-2}K^{-1}$ and h=150 $Wm^{-2}K^{-1}$, respectively. All other parameters remain the same. It is found that changing the convective heat transfer coefficient completely changes the nature of the heat removal curves. The non-monotonic behavior of total heat removed seen in Figure 9 is not seen any longer in Figures 10(a) and 10(b). It is found instead that the total heat removed increases (Figure 10(a)) or decreases (Figure 10(b)) monotonically with porosity when the convective heat transfer coefficient is lower or higher, respectively, than the value considered in Figure 9. This is mainly because increasing h reduces the convective resistance at the fin surface, R_{surf}, as shown in Figure 2 without impacting the advective resistance R_{adv}. As a result, more heat is drawn conductively through while the advective component remains the same. As a result, the total heat removed becomes dominated by the conductive component, and, thus shows a decreasing trend with porosity, as seen in Figure 10(b). A similar explanation may be provided for the impact of reducing h on heat removal rates.

Figure 10 shows that when the convective heat transfer is very small, such as in natural convection conditions around the fin, it is best to design the fin to be as porous as possible, within other constraints such as structural integrity. On the other hand, as shown in Figure 10(b), under forced convective conditions around the fin, having a porous fin is not beneficial at all, since the improvement in advective heat removal with increasing porosity is completely overwhelmed by the reduction in conductive heat removal as porosity increases.

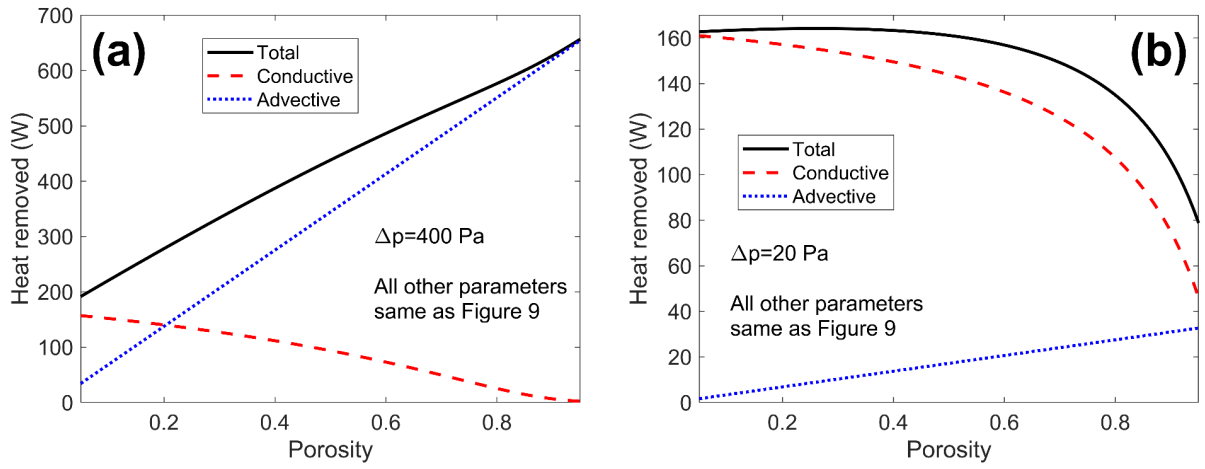

Figure 11. Heat removal rate as a function of fin porosity for (a) Δp=400 Pa and (b) Δp=20 Pa. Other parameters are the same as Figure 9. Total heat removed as well as the conductive and advective components are plotted.

As another illustration of the impact of design parameters on how the heat removal rate varies with porosity, the same baseline case as Figure 9 is considered again, but with different values of the imposed pressure gradient. In contrast with the baseline value of Δp=100 Pa, Figures 11(a) and 11(b) plot heat removal curves as functions of porosity for Δp=400 Pa and Δp=20 Pa, respectively. It is found that while the greater pressure difference results in a monotonically increasing heat removal rate as a function of porosity, the lower pressure difference completely reverses the trend, resulting in a monotonically decreasing heat removal rate as a function of porosity. This is mainly because changing the pressure difference affects the advective resistance R_{adv} without affecting any other resistances in the problem, thereby making the total heat removal more dominant or less dominant by advective or conductive heat removal, respectively, at larger or smaller pressure differences.

Similar to the effect of the convective heat transfer coefficient examined in Figure 10, this analysis shows that determining whether a porous fin is beneficial or not and, if so, selecting the best

porosity depends strongly on the available pressure difference that drives the porous flow. For very large pressure difference, the larger the porosity, the more effective is the fin. In contrast, for very small pressure difference, there is no benefit of using a porous fin.

Whether an optimal value of the porosity exists, and if so, determining that value can be addressed by examining the derivative of the total heat removed with respect to the porosity. Differentiating equation (16) and setting to zero results in

$$\frac{\mathrm{K}\cdot\rho_f c_f\cdot\Delta p}{\mu\cdot\ln\left(\frac{R_0+L}{R_0}\right)}=\left(k_f-k_s\right)\left(\frac{\partial\theta}{\partial\xi}\right)_{\xi=1}+k_{eff}\frac{\partial}{\partial\phi}\left[\left(\frac{\partial\theta}{\partial\xi}\right)_{\xi=1}\right] \tag{28}$$

The root of equation (28), if one exists between 0 and 1 is the optimal porosity for maximizing heat removal by the fin.

Effect of tip conditions

Similar to a traditional, non-porous fin, the nature of the convective boundary conditions at the fin tip is expected to influence the temperature distribution in the porous fin. The two key non-dimensional parameters that describe thermal conditions at the fin tip are the tip Biot number Bi_{tip} and tip temperature $\theta_{\infty,tip}$. As discussed in Section 3, specific values of these parameters transform the general problem considered here into special cases, such as an adiabatic tip or an isothermal tip.

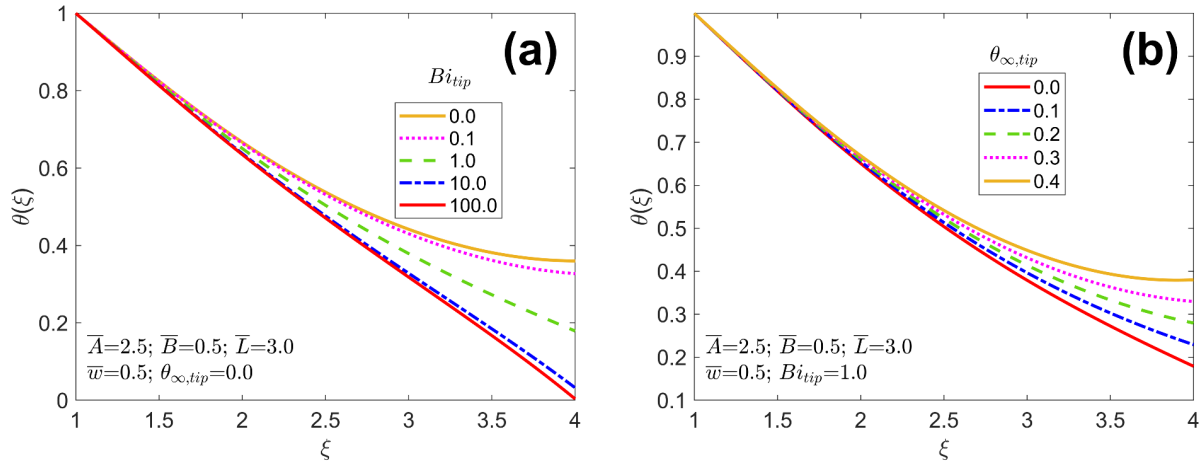

Figure 12. Effect of fin tip conditions: Fin temperature distribution for (a) multiple values of Bi_{tip}*, with* $\theta_{\infty,tip} = 0.0$*, (b) multiple values of* $\theta_{\infty,tip}$ *with* $Bi_{tip} = 1.0$*. Other problem parameters are* $\bar{A} = 2.5$*,* $\bar{B} = 0.5$*,* $\bar{L} = 3.0$ *and* $\bar{w} = 0.5$*.*

In order to examine the impact of Bi_{tip} and $\theta_{\infty,tip}$ on thermal response of the fin, the fin temperature distribution is plotted for multiple values of Bi_{tip} and $\theta_{\infty,tip}$ in Figures 12(a) and 12(b), respectively. Figure 12(a) is plotted for $\theta_{\infty,tip} = 0.0$, while Figure 12(b) is plotted for $Bi_{tip} = 1.0$. Other non-dimensional parameters are $\bar{A} = 2.5$, $\bar{B} = 0.5$, $\bar{L} = 3.0$ and $\bar{w} = 0.5$. Figure 12(a) shows that for $Bi_{tip} = 0.0$, the fin is, in general, the hottest. This, however, does not imply greater heat removal, since all curves in Figure 12(a) have nearly the same slope at $\xi = 1$. Note that $Bi_{tip} = 0.0$ renders the fin tip adiabatic, resulting in no heat removal from the end of the fin, as confirmed by the flat nature of the $Bi_{tip} = 0.0$ curve at $\xi = \bar{L}$. As Bi_{tip} increases, the fin temperature curves shift downwards and the slope at the fin tip becomes larger in magnitude, indicating increased heat loss from the fin tip. However, the effect of fin tip conditions does not extend throughout the fin, and, in particular, does not influence heat removal from the base. For very large value of Bi_{tip}, Figure 12(a) shows that the fin tip temperature becomes very close to $\theta_{\infty,tip}$, approaching isothermal fin tip conditions. Note that the tip temperature for both $Bi_{tip} =$

10.0 and $Bi_{tip} = 100.0$ curves is close to $\theta_{\infty,tip}$, indicating that both values of the Biot number are close to isothermal conditions.

The impact of $\theta_{\infty,tip}$ is examined in Figure 12(b). In this case, $Bi_{tip} = 1.0$, which is a reasonably low value. This is the reason why the temperature curves in Figure 12(b) do not reach $\theta_{\infty,tip}$ at the tip. Nevertheless, the lower the value of $\theta_{\infty,tip}$, the lower is the temperature curve in general. Note that for relatively large value of $\theta_{\infty,tip} = 0.4$, the temperature curve actually reaches a minima within the fin and then rises towards the fin tip, indicating the some parts of the fin may be cooler than the fin tip. This only occurs for large value of $\theta_{\infty,tip}$, which is likely unrealistic, since the fin tip is unlikely to be hotter than the ambient around the fin. In most cases, the two are expected to be the same, and, therefore, $\theta_{\infty,tip} = 0.0$ is the most likely scenario.

Note in both Figures 12(a) and 12(b), changing the tip conditions, i.e., Bi_{tip} and $\theta_{\infty,tip}$, does not appreciably change the slope of the temperature at the base of the fin. This indicates the conductive heat removed by the fin is largely independent of the tip conditions. Since the convective heat removal also does not depend on Bi_{tip} and $\theta_{\infty,tip}$, therefore, under the conditions considered here, fin performance is largely independent of the fin tip. This may be because of the relatively large length of the fin considered here. For a shorter fin, it can be seen that increasing the tip Biot number significantly improves the non-dimensional fin heat removal.

Conclusions

The key contributions of this work include the thermal analysis of a radial porous fin in which heat removal is aided by radial pressure-driven flow instead of natural convection flow considered in past papers, and the identification of key conduction-vs-advection trade-offs in fin design.

Under a certain set of parameters, it is shown that there exists a fin porosity that maximizes heat removal rate. Under certain other set of parameters, it is shown that a porous fin may not offer any benefits at all over a non-porous fin of the same geometry. These insights may be helpful to choosing whether to use a porous fin or not in a given heat transfer problem, and if so, the correct porosity to choose.

Non-dimensional curves presented in this work improve the general understanding of extended surface heat transfer, particularly in the context of porous fins. Such curves may be useful for the general design of heat transfer systems.

It must be noted that this work analyzes only the heat transfer aspects of a porous fin. A highly porous fin is also light-weight. Weight reduction may be desirable for certain applications, but is comes at the cost of reduced ability to withstand mechanical loads. For applications where weight and load bearing capability are important, such mechanical considerations must also be accounted for in fin design and optimization, in addition to the thermal analysis presented here. In addition, the pumping power needed to sustain the pressure-driven flow, which is not considered here, may be important in certain problems.

While the porous flow in this work is assumed to be driven by a pressure gradient, other fluid flow mechanisms, such as electro-osmotic flow can be easily analyzed within the same framework as the one presented here. The present work assumes negligible natural convection of the porous fluid within the fin. Radiative effects have also been neglected due to a reasonably small temperature difference. Thermal properties of the fin material and fluid are assumed to be independent of temperature. Porous fluid flow is assumed to be Newtonian and laminar, and with constant permeability. While these assumptions are reasonable for a wide range of applications, in other problems, several of these assumptions can potentially be relaxed, in which case, the use

of numerical techniques to solve the resulting equations may be necessary. Nevertheless, several important trade-offs identified here may persist in such scenarios.

References

[1] A.D. Kraus, A.M. Aziz, J.R. Welty, *Extended Surface Heat Transfer*, John Wiley, New York, 2002.

[2] R.L. Webb, B. Sunden, N.-H. Kim, *Principles of Enhanced Heat Transfer*, Routledge, Boca Raton, 2005.

[3] R.J. McGlen, R. Jachuck, S. Lin, 'Integrated thermal management techniques for high power electronic devices,' *Appl. Therm. Eng.*, **24**, pp. 1143-1156, 2004. DOI: 10.1016/j.applthermaleng.2003.12.029

[4] A. Mostafavi, M. Parhizi, A. Jain, 'Theoretical modeling and optimization of fin-based enhancement of heat transfer into a phase change material,' *Int. J. Heat Mass Transf.*, **145**, pp: 118698:1-10, 2019. DOI: 10.1016/j.ijheatmasstransfer.2019.118698.

[5] H.H. Pennes, 'Analysis of Tissue and Arterial Blood Temperatures in the Resting Human Forearm,' *J. Appl. Physiol.*, **1**, pp. 93-122, 1948. DOI: 10.1152/jappl.1948.1.2.93

[6] S.-H. Park, J.H. Jeong, 'Analytical fin efficiency model for open-cell porous metal fins based on Kelvin cell assumption,' *Int. J. Heat Mass Transf.*, **196**, pp. 123283, 2022. DOI: 10.1016/j.ijheatmasstransfer.2022.123283.

[7] S. Kiwan, M.A. Al-Nimr, 'Using Porous Fins for Heat Transfer Enhancement,' *ASME J. Heat Mass Transf.*, **123**, pp. 79-795, 2001. DOI: 10.1115/1.1371922

[8] M. Torabi, H. Yaghoobi, 'Series solution for convective-radiative porous fin using differential transformation method,' *J. Porous Media*, **16**, pp. 341–349, 2013. DOI: 10.1615/JPorMedia.v16.i4.60

[9] D.A. Nield, A. Bejan, *Convection in Porous Media*, 4th Ed.., Springer, 2013.

[10] M. Kaviany, *Principles of Heat Transfer in Porous Media*, 2nd Ed., Springer New York, NY, 1995. DOI: 10.1007/978-1-4612-4254-3

[11] F.M. White, *Viscous Fluid Flow*, 3rd Ed., McGraw Hill, 2005.

[12] S. Saedodin, M. Shahbabaaei, 'Thermal Analysis of Natural Convection in Porous Fins with Homotopy Perturbation Method (HPM),' *Arab. J. Sci. Eng.*, **38**, pp. 2227-2231, 2013. DOI: 10.1007/s13369-013-0581-6

[13] T. Zhao, H. Tian, L. Shi T. Chen, X. Ma, M. Atik, G. Shu, 'Numerical analysis of flow characteristics and heat transfer of high-temperature exhaust gas through porous fins,' *Appl. Therm. Eng.*, **165**, pp. 114612, 2020. DOI: 10.1016/j.applthermaleng.2019.114612

[14] H. Kahalerras, N. Targui, 'Numerical analysis of heat transfer enhancement in a double pipe heat exchanger with porous fins,' *Int. J. Numer. Methods for Heat & Fluid Flow*, **18**, pp., 593-617, 2008, DOI: 10.1108/09615530810879738 2008

[15] S. Kiwan, 'Thermal Analysis of Natural Convection Porous Fins,' *Transport in Porous Media*, **67**, pp. 17-29, 2007. DOI: 10.1007/s11242-006-0010-3

[16] R. Das, 'Forward and inverse solutions of a conductive, convective and radiative cylindrical porous fin,' *Energy Conv. Management*, **87**, pp. 96-106, 2014. DOI: 10.1016/j.enconman.2014.06.096

[17] M. Hatami, D.D. Ganji, 'Thermal performance of circular convective–radiative porous fins with different section shapes and materials,' *Energy Conv. Management*, **76**, pp. 185-193, 2013. DOI: 10.1016/j.enconman.2013.07.040

[18] M. Turkyilmazoglu, 'Efficiency of heat and mass transfer in fully wet porous fins: Exponential fins versus straight fins,' *Int. J. Refrig.*, **46**, pp. 158-164, 2014. DOI: 10.1016/j.ijrefrig.2014.04.011

[19] D. S. Kumar, S. Jayavel, 'Optimization of porous fin location and investigation of porosity and permeability effects on hydro-thermal behavior of rectangular microchannel heat sink,' *Int.*

Communic. Heat Mass Transf., **129**, pp. 105737, 2011. DOI: 10.1016/j.icheatmasstransfer.2021.105737

[20] B. Kundu, D. Bhanja, K.-S. Lee, 'A model on the basis of analytics for computing maximum heat transfer in porous fins,' *Int. J. Refrig.*, **55**, pp. 7611-7622, 2012. DOI: 10.1016/j.ijheatmasstransfer.2012.07.069

[21] M. Hatami, A. Hasanpour, D.D. Ganji, 'Heat transfer study through porous fins (Si_3N_4 and Al) with temperature-dependent heat generation,' *Energy Conv. Management*, **74**, pp. 9-16, 2013. DOI: 10.1016/j.enconman.2013.04.034

[22] J. Ma, Y. Sun, B. Li, H. Chen, 'Spectral collocation method for radiative–conductive porous fin with temperature dependent properties,' *Energy Conv. Management*, **111**, pp. 279-288, 2016. DOI: 10.1016/j.enconman.2015.12.054

[23] M. Turkyilmazoglu, 'Exact Heat-Transfer Solutions to Radial Fins of General Profile,' *J. Thermophys. Heat Transf.*, **30**, pp. 1-5, 2015. DOI: 10.2514/1.T4555

[24] M. Turkyilmazoglu, 'Thermal management of parabolic pin fin subjected to a uniform oncoming airflow: optimum fin dimensions,' *J. Therm. Anal. Calorimetry*, **143**, pp. 3731-3739, 2021. DOI: 10.1007/s10973-020-10382-x

[25] M. Turkyilmazoglu, 'Prescribed Temperature Profiles of Longitudinal Convective-Radiative Fins Subject to Axially Distributed Thermal Conductivities,' *Arabian J. Sci. Eng.*, **47**, pp. 15689–15703, 2022. DOI: 10.1007/s13369-022-06710-y

[26] F.P. Incropera, D.P. DeWitt, T.L. Bergman, A.S. Levine, *Fundamentals of Heat and Mass Transfer*, John Wiley & Sons, 6th Ed., 2006.

[27] A. Jain, M. Parhizi, L. Zhou, G. Krishnan, 'Imaginary eigenvalues in multilayer one-dimensional thermal conduction problem with linear temperature-dependent heat generation,' *Int. J. Heat Mass Transf.*, **170**, pp. 120993:1-10, 2021. DOI: 10.1016/j.ijheatmasstransfer.2021.120993.

[28] A. Jain, S. McGinty, G. Pontrelli, L. Zhou, 'Theoretical Modeling of Endovascular Drug Delivery into a Multilayer Arterial Wall from a Drug-Coated Balloon,' *Int. J. Heat Mass Transf.*, **187**, pp. 122572:1-17, 2022. DOI: 10.1016/j.ijheatmasstransfer.2022.122572

[29] E.B. Nauman, *Chemical Reaction Design, Optimization and Scaleup*, 2nd Ed., John, Wiley & Sons, Hoboken, NJ, 2008. ISBN: 9780470282069

[30] E. Augeraud-Véron, C. Choquet, É. Comte, 'Optimal Control for a Groundwater Pollution Ruled by a Convection–Diffusion–Reaction Problem,' *J. Optimiz. Theory & Appl.*, **173**, pp. 941–966, 2017. DOI: 10.1007/s10957-016-1017-8

[31] M. Abramowitz, I. Stegun, 'Handbook of Mathematical Functions,' United States Department of Commerce National Bureau of Standards, 1964.

CHAPTER 3: TRANSIENT THERMAL MANAGEMENT CHARACTERISTICS OF A POROUS FIN WITH RADIALLY OUTWARDS FLUID FLOW

Problem Definition

Consider the transient thermal transport problem associated with heat removal from a hot, constant temperature surface by a porous fin. This problem is defined in cylindrical coordinates, in which, a radial fin of constant thickness removes heat from a hot, annular cylinder, as shown in the schematic presented in Figure 13(a). In addition to conventional conductive heat removal through the fin, its porous nature additionally enables advective heat removal due to radially outwards porous flow through the fin. Such a flow could be driven by, for example, a pressure gradient between fluid inside the cylinder and the tip of the fin. Other flow mechanisms such as electro-osmotic flow may also be possible but are not explicitly considered here. Both conductive and advective heat removal mechanisms are closely related to the fin porosity, since porosity affects both effective thermal conductivity that drives conductive heat removal, as well as the radially outwards flow field that drives advective heat removal.

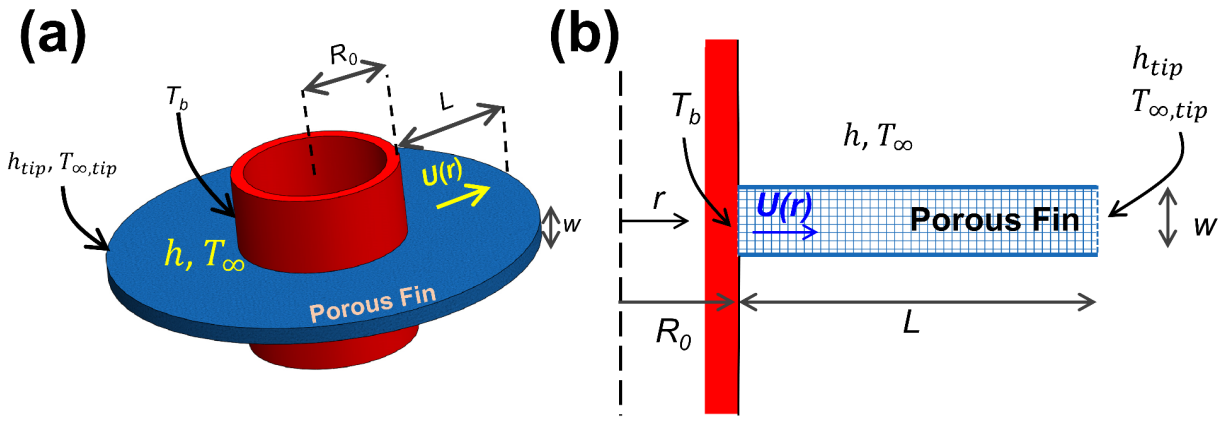

Figure 13. (a) Schematic and (b) Cross-section of a porous fin with pressure gradient driven radially outwards flow through the fin that provides an additional mechanism for heat removal from the fin base.

While a previous work has analyzed this problem in steady state [22], there are several practical applications where heat transfer by the fin occurs only over a limited time. An example includes thermal management of a semiconductor chip or a Li-ion battery, where, in both cases, heat generation occurs only for a relatively short period of time, during which, the fin may not reach steady state. As another example, fin-based enhancement of latent energy storage in a phase change material (PCM) around a hot source is also a transient process, depending on how long the hot source, such as solar heat, is available. It is important to develop a transient thermal model to predict porous fin performance as a function of time, since previously developed steady state models do not address this need.

A schematic of the porous fin is shown schematically in Figure 13(a), along with a cross-section view in Figure 13(b). A transverse radial fin is attached to the outer surface of a hot hollow cylinder of radius R_0. The outer radius and width of the fin are $R_0 + L$ and w, respectively. The fin base is assumed to remain at a fixed temperature T_0. The fin is composed of a porous material and sealed on the top and bottom surfaces, so that a pressure gradient driven radially outwards

fluid flow in established from the base of the fin, $r = R_0$ to its tip $r = R_0 + L$. Along the length of the fin, heat loss to the surroundings occurs through convective heat transfer, represented by a convective heat transfer coefficient h along with freestream temperature T_∞. For generality, separate values of convective heat transfer coefficient h_{tip} and freestream temperature $T_{\infty,tip}$ are assumed at the fin tip. Thermal conductivity, heat capacity and density are denoted by k, c and ρ, respectively, with subscripts s and f for the solid and fluid components of the fin, respectively. Porosity and permeability of the fin material are denoted by ϕ and K, respectively. The entire fin is assumed to be initially at a temperature T_∞. For a given time period, the interest is in determining the heat removed by the fin through both conductive and advective mechanisms, and to develop an understanding of how to design the fin, for example, how to choose the fin porosity in order to maximize heat removal over a given time period. Such a performance evaluation of the fin first requires determining the transient temperature field in the fin.

A number of assumptions are made in order to carry out this analysis. The fin is assumed to be axisymmetric. All thermal and flow properties, as well as those associated with the porous material, such as porosity and permeability are assumed to be constant and uniform. While the thermal field is transient, the flow field is assumed to be steady. Assuming the flow field to be laminar and Darcian, an expression for the steady velocity field may be derived as follows [22, 24]

$$U(r) = \frac{\mathrm{K} \cdot \Delta p}{\mu \cdot \ln\left(\frac{R_0 + L}{R_0}\right) \cdot r} \tag{1}$$

Note that the $1/r$ dependence of the velocity field helps conserve mass.

Based on the assumptions listed above, the temperature field in the porous is spatially one-dimensional, in the radial direction only. The general energy conservation equation that governs the transient temperature field $T(r,t)$ may be written as

$$\frac{k_{eff}}{r}\frac{\partial}{\partial r}\left(r\frac{\partial T}{\partial r}\right)-\frac{\phi\rho_f c_f}{r}\frac{\partial}{\partial r}(r\cdot T\cdot U(r))-\frac{h}{w}(T-T_\infty)=\rho_f c_f\frac{\partial T}{\partial t} \quad (2)$$

where the three terms on the left hand side represent diffusion, advection and convective heat removal, respectively, in an infinitesimal fin element. The boundary conditions and initial condition for the temperature field are

$$T=T_b \quad (r=R_0) \quad (3)$$

$$-k_{eff}\frac{\partial T}{\partial r}=h_{tip}\left(T-T_{\infty,tip}\right) \quad (r=R_0+L) \quad (4)$$

$$T=T_\infty \quad (t=0) \quad (5)$$

where k_{eff} is the effective thermal conductivity of the porous medium. In general, k_{eff} may be obtained based on an appropriate average of the solid and fluid thermal conductivities, in which, the porosity plays a key role. A commonly used weighted average based on porosity, i.e., $k_{eff}=\phi k_f+(1-\phi)k_s$ [24] is adopted in this work.

In order to simplify this problem and to ensure the generality of the solution derived, it is cast in non-dimensional form using the following variables and parameters:

$$\xi = \frac{r}{R_0}; \tau = \frac{k_{eff}t}{\rho_f c_f R_0^2}; \theta = \frac{T - T_\infty}{T_b - T_\infty}; \bar{A} = \frac{\mathrm{K} \cdot \rho_f c_f \cdot \Delta p \cdot \phi}{\mu \cdot \ln\left(\frac{R_0 + L}{R_0}\right) k_{eff}}; \bar{B} = \frac{hR_0^2}{k_{eff} w};\ \bar{L} = \frac{L}{R_0}; Bi_{tip} = \frac{h_{tip} R_0}{k_{eff}};\ \theta_{\infty,tip} = \frac{T_{\infty,tip} - T_\infty}{T_b - T_\infty};\ \bar{w} = \frac{w}{R_0} \tag{6}$$

This results in the following non-dimensional transient energy conservation equation

$$\frac{1}{\xi}\frac{\partial}{\partial \xi}\left(\xi \frac{\partial \theta}{\partial \xi}\right) - \frac{\bar{A}}{\xi}\frac{\partial \theta}{\partial \xi} - \bar{B}\theta = \frac{\partial \theta}{\partial \tau} \tag{7}$$

Equation (7) represents a transient Convection-Diffusion-Reaction (CDR) equation [25-27]. The non-dimensional temperature field is also subject to the following boundary conditions and initial condition

$$\theta = 1 \qquad (\xi = 1) \tag{8}$$

$$-\frac{\partial \theta}{\partial \xi} = Bi_{tip}\left(\theta - \theta_{\infty,tip}\right) \qquad (\xi = 1 + \bar{L}) \tag{9}$$

$$\theta = 0 \qquad (\tau = 0) \tag{10}$$

Solution of the Problem

Due to the non-homogeneity appearing in the boundary condition given by equation (8), one may first substitute $\theta(\xi, \tau) = v(\xi) + u(\xi, \tau)$, where v and u are the steady state and transient components, respectively, of the temperature distribution. By inserting this form of θ in the

governing equation and boundary conditions, one may write the following differential equation for $v(\xi)$:

$$\frac{1}{\xi}\frac{\partial}{\partial\xi}\left(\xi\frac{\partial v}{\partial\xi}\right)-\frac{\bar{A}}{\xi}\frac{\partial v}{\partial\xi}-\bar{B}v=0 \tag{11}$$

subject to the following boundary conditions:

$$v=1 \qquad (\xi=1) \tag{12}$$

$$-\frac{\partial v}{\partial\xi}=Bi_{tip}\left(v-\theta_{\infty,tip}\right) \qquad (\xi=1+\bar{L}) \tag{13}$$

The $v(\xi)$ problem is indeed the steady-state problem for the porous fin with radially outwards flow, which has been solved in a recent paper [22]. The solution for the problem is given by [22]

$$v(\xi)=\xi^{\bar{A}/2}\left[c_1 I_{\bar{A}/2}\left(\sqrt{\bar{B}}\xi\right)+c_2 K_{\bar{A}/2}\left(\sqrt{\bar{B}}\xi\right)\right] \tag{14}$$

where the coefficients c_1 and c_2 are obtained on the basis of the boundary conditions. *I* and *K* are modified Bessel functions of the first and second kind, respectively [28]. Expressions for c_1 and c_2 are available from the recent steady-state analysis [22] and are not reproduced here for brevity.

The differential equation governing the rest of the temperature field, $u(\xi,\tau)$ is given by

$$\frac{1}{\xi}\frac{\partial}{\partial\xi}\left(\xi\frac{\partial u}{\partial\xi}\right)-\frac{\bar{A}}{\xi}\frac{\partial u}{\partial\xi}-\bar{B}u=\frac{\partial u}{\partial\tau} \tag{15}$$

subject to

$$u=0 \qquad (\xi=1) \tag{16}$$

$$-\frac{\partial u}{\partial\xi}=Bi_{tip}\cdot u \qquad (\xi=1+\bar{L}) \tag{17}$$

$$u(\xi,\tau)=-v(\xi) \qquad (\tau=0) \tag{18}$$

Note that the $u(\xi,\tau)$ problem is free of non-homogeneities in the governing equation as well as the boundary conditions. Therefore, a solution may be derived using the method of separation of variables. Substituting $u(\xi,\tau)=\xi^{\frac{\bar{A}}{2}}\cdot f(\xi)\cdot g(\tau)$ and separating the equations for $f(\xi)$ and $g(\tau)$, one may derive the following form of the solution

$$u(\xi,\tau)=\sum_{m=1}^{\infty}\xi^{\frac{\bar{A}}{2}}\cdot s_m\left(J_{\frac{\bar{A}}{2}}(\omega_m\xi)+c_{2,m}\cdot Y_{\frac{\bar{A}}{2}}(\omega_m\xi)\right)e^{-\lambda_m^2\tau} \tag{19}$$

where $\omega_m=\sqrt{\lambda_m^2-\bar{B}}$, and J and Y are Bessel functions of the first and second kind, respectively. The order of both Bessel functions that appear in the solution is $\bar{A}/2$. The eigenvalues λ_m and coefficient $c_{2,m}$ may be determined by applying boundary conditions given by equations (16) and (17). Rearrangement of the resulting equations may be shown to result in the following eigenequation:

$$\left(\sqrt{\lambda^2-\bar{B}}\,Y_{\frac{\bar{A}}{2}-1}\left[(1+\bar{L})\sqrt{\lambda^2-\bar{B}}\right]+Bi_{tip}\cdot Y_{\frac{\bar{A}}{2}}\left[(1+\bar{L})\sqrt{\lambda^2-\bar{B}}\right]\right)J_{\frac{\bar{A}}{2}}\left[\sqrt{\lambda^2-\bar{B}}\right] \tag{20}$$

$$-\left(\sqrt{\lambda^2-\bar{B}}\,J_{\frac{\bar{A}}{2}-1}\left[(1+\bar{L})\sqrt{\lambda^2-\bar{B}}\right]+Bi_{tip}\right.$$

$$\left.\cdot J_{\frac{\bar{A}}{2}}\left[(1+\bar{L})\sqrt{\lambda^2-\bar{B}}\right]\right)J_{\frac{\bar{A}}{2}}\left[\sqrt{\lambda^2-\bar{B}}\right]=0$$

Further, it can be found from equation (16) that $c_{2,m}=-\frac{J_{\frac{\bar{A}}{2}}(\omega_m)}{Y_{\frac{\bar{A}}{2}}(\omega_m)}$. Therefore, the solution for $u(\xi,\tau)$ may be written as

$$u(\xi,\tau)=\sum_{m=1}^{\infty}\xi^{\frac{\bar{A}}{2}}\cdot s_m\left(J_{\frac{\bar{A}}{2}}(\omega_m\xi)-\frac{J_{\frac{\bar{A}}{2}}(\omega_m)}{Y_{\frac{\bar{A}}{2}}(\omega_m)}\cdot Y_{\frac{\bar{A}}{2}}(\omega_m\xi)\right)e^{-\lambda_m^2\tau} \tag{21}$$

The last remaining set of coefficients, s_m may be determined by using the initial condition given by equation (18) in conjunction with the principle of orthogonality of the eigenfunctions. Note that due to the appearance of the advective term in the governing equation, the principle of orthogonality differs slightly from that for pure-diffusion problems. Specifically, as shown in prior work on a CDR problem [29], a weighing function $\xi^{1-\frac{\bar{A}}{2}}$ must be included in the expression for orthogonality of eigenfunctions. Equation (18) is inserted into (19), followed by multiplying both sides by $\xi^{1-\frac{\bar{A}}{2}}\left(J_{\frac{\bar{A}}{2}}(\omega_{m'}\xi)+c_{2,m'}\cdot Y_{\frac{\bar{A}}{2}}(\omega_{m'}\xi)\right)$ and integrating from $\xi=1$ to $\xi=1+\bar{L}$. Based on orthogonality, this results in elimination of all terms except one, a formal proof for which is available in the literature [29]. This leads to the following expression for s_m

$$s_m = \frac{\int_1^{1+\bar{L}} -v_m(\xi)\left(J_{\frac{\bar{A}}{2}}(\omega_m\xi) + c_{2,m}Y_{\frac{\bar{A}}{2}}(\omega_m\xi)\right)\xi^{1-\frac{\bar{A}}{2}}\,d\xi}{\int_1^{1+\bar{L}} \xi\left(J_{\frac{\bar{A}}{2}}(\omega_m\xi) + c_{2,m}Y_{\frac{\bar{A}}{2}}(\omega_m\xi)\right)^2 d\xi} \tag{22}$$

Note that the denominator in equation (22) is the norm of the eigenfunctions of this problem.

This completes the derivation of the solution of the problem. The final solution for the temperature distribution on the fin is given by equations (14) and (21), along with equations (20) and (22).

Based on the temperature distribution derived here, one may write the following expression for the dimensional rate of heat removal from the fin base as a function of time

$$q(t) = \left(-k_{eff}\left(\frac{\partial T}{\partial r}\right)_{r=R_0} + \phi\rho_f c_f \cdot \mathrm{U}(R_0)(T_b - T_\infty)\right)2\pi R_0 w \tag{23}$$

Note that the first and second terms in the expression for $q(t)$ represent conductive and advective rates of heat removal, respectively.

Based on the instantaneous rate of heat removal derived above, the following expression for the non-dimensional heat removal rate may be written

$$\bar{q}(\tau) = \frac{q(t)}{k_{eff}(T_b - T_\infty)2\pi w}$$

$$= \bar{A} - \sqrt{\bar{B}}\left(c_1 I_{\frac{\bar{A}}{2}-1}\left(\sqrt{\bar{B}}\right) - c_2 K_{\frac{\bar{A}}{2}-1}\left(\sqrt{\bar{B}}\right)\right) \tag{24}$$

$$+ \sum_{m=1}^{\infty} s_m \omega_m \left(J_{\frac{\bar{A}}{2}-1}(\omega_m) - \frac{J_{\frac{\bar{A}}{2}}(\omega_m)}{Y_{\frac{\bar{A}}{2}}(\omega_m)} \cdot Y_{\frac{\bar{A}}{2}-1}(\omega_m)\right) e^{-\lambda_m^2 \tau}$$

While equation (24) represents the instantaneous rate of heat removal at any given time, an averaged rate of heat removal up to a given time may be of practical interest for applications in which a finite amount of time is available for heat transfer. One may derive

$$\bar{q}_{avg}(\tau) = \frac{\int_0^t q(t^*)dt^*}{t}$$

$$= \bar{A} - \sqrt{\bar{B}}\left(c_1 I_{\frac{\bar{A}}{2}-1}\left(\sqrt{\bar{B}}\right) - c_2 K_{\frac{\bar{A}}{2}-1}\left(\sqrt{\bar{B}}\right)\right)$$

$$+ \sum_{m=1}^{\infty} s_m \omega_m \left(J_{\frac{\bar{A}}{2}-1}(\omega_m) - \frac{J_{\frac{\bar{A}}{2}}(\omega_m)}{Y_{\frac{\bar{A}}{2}}(\omega_m)} \cdot Y_{\frac{\bar{A}}{2}-1}(\omega_m)\right) \frac{1 - e^{-\lambda_m^2 \tau}}{\lambda_m^2 \tau}$$

(25)

Fin Transient Performance Parameters

One may define the fin effectiveness to be the ratio of total heat removal rate by the fin and total heat that would be removed directly from the base in the absence of the fin

$$\eta(t) = \frac{\left(-k_{eff}\left(\frac{\partial T}{\partial r}\right)_{r=R_0} + \phi\rho_f c_f \cdot \mathrm{U}(R_0)(T_b - T_\infty)\right) 2\pi R_0 w}{2\pi R_0 w h (T_b - T_\infty)} \tag{26}$$

which can be shown to result in

$$\eta(\tau) = \frac{1}{Bi}\left[\bar{A} - \sqrt{\bar{B}}\left(c_1 I_{\frac{\bar{A}}{2}-1}\left(\sqrt{\bar{B}}\right) - c_2 K_{\frac{\bar{A}}{2}-1}\left(\sqrt{\bar{B}}\right)\right) + \sum_{m=1}^{\infty} s_m \omega_m \left(J_{\frac{\bar{A}}{2}-1}(\omega_m) - \frac{J_{\frac{\bar{A}}{2}}(\omega_m)}{Y_{\frac{\bar{A}}{2}}(\omega_m)} \cdot Y_{\frac{\bar{A}}{2}-1}(\omega_m)\right) e^{-\lambda_m^2 \tau}\right] \tag{27}$$

Note that the fin effectiveness is a function of time, since the heat removal rate by the fin changes over time. It is expected that the fin effectiveness will be very high at early times, owing to large conductive heat removal due to large temperature gradient between the base and the fin.

In addition, it is also of interest to define a fin effectiveness on the basis of comparison of porous fin performance with a non-porous fin of the same geometry and operating under identical conditions. Such a comparison is pertinent in order to understand whether a porous fin offers improved thermal performance than its non-porous equivalent. While porosity in the fin offers advective heat removal that is absent from the non-porous fin, yet, the porous fin has lower effective thermal conductivity, implying that its conductive heat removal may be lower than the non-porous fin. Therefore, it is important to compare the total heat removal by both porous and non-porous fins. This may be done by defining the porous fin effectiveness as the ratio of heat

removal by the two fins. Similar to fin effectiveness, the porous fin effectiveness is also a function of time

$$\eta_{porous}(\tau) = \frac{\bar{A} - \sqrt{\bar{B}}\left(c_1 I_{\frac{\bar{A}}{2}-1}\left(\sqrt{\bar{B}}\right) - c_2 K_{\frac{\bar{A}}{2}-1}\left(\sqrt{\bar{B}}\right)\right) + \sum_{m=1}^{\infty} s_m \omega_m \left(J_{\frac{\bar{A}}{2}-1}(\omega_m) - \frac{J_{\frac{\bar{A}}{2}}(\omega_m)}{Y_{\frac{\bar{A}}{2}}(\omega_m)} \cdot Y_{\frac{\bar{A}}{2}-1}(\omega_m)\right) e^{-\lambda_m^2 \tau}}{-\sqrt{\bar{B}_s}\left(c_{1,s} I_1\left(\sqrt{\bar{B}_s}\right) - c_{2,s} K_1\left(\sqrt{\bar{B}_s}\right)\right) - \sum_{m=1}^{\infty} s_{m,s} \omega_{m,s} \left(J_1(\omega_{m,s}) - \frac{J_0(\omega_{m,s})}{Y_0(\omega_{m,s})} \cdot Y_1(\omega_{m,s})\right) e^{-\lambda_m^2 \tau}} \tag{28}$$

Where, in the denominator, $\omega_{m,s} = \sqrt{\lambda_{m,s}^2 - \bar{B}_s}$, $\bar{B}_s = \frac{hR_0^2}{k_s w}$ and $\lambda_{m,s}$ are obtained from roots of the eigenequation given by equation (20) while using $\bar{B}_s$ instead of $\bar{B}$ and $\bar{A} = 0$ in order to model the non-porous fin.

Results and Discussion

In order to highlight key features of this transient thermal problem, the transient temperature field in the fin is determined first, followed by computation of heat removal and other performance parameters of the fin. In each case, the transient behavior of fin performance is of particular interest.

Number of terms needed

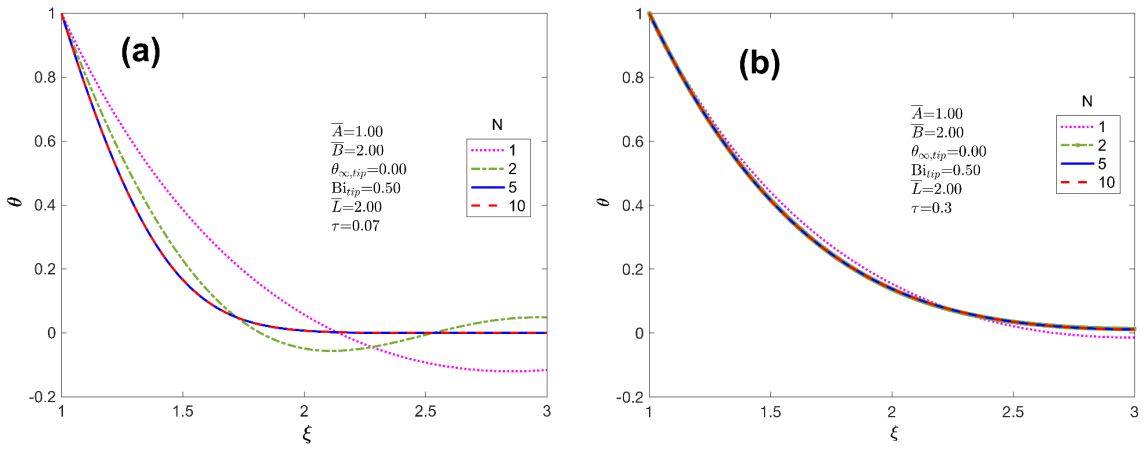

Figure 14.Figure 2. Effect of number of eigenvalues considered in the analytical solution: Temperature distribution along the fin at (a) τ=0.07, (b) τ=0.30. Curves corresponding to different number of eigenvalues are presented. Parameter values are $\bar{A}$=1.0, $\bar{B}$=1

Firstly, due to the infinite series nature of the transient temperature distribution derived in this work, it is important to determine the number of eigenvalues that must be accounted for in computations. This helps determine a reasonable balance between accuracy and computational time. In general, the greater the number of terms considered, the more accurate is the computed temperature, but at a greater computational cost. Once converged, increasing the number of terms further offers only a negligible improvement in accuracy while continuing to increase computational cost. Therefore, it is of interest to determine the minimum number of terms needed

for a specific computation. This is often done in terms of convergence analysis. In the present case, temperature distribution along the fin is computed at two specific times, while including different number of eigenvalues, denoted by N. Results are presented in Figure 14, which shows that the computed temperature distribution with $N = 5$ and $N = 10$ terms are practically identical at both times. Therefore, the use of five terms is found to be sufficient at the two times considered in Figure 14. Since the number of terms needed for convergence of an eigenfunction-based series solution usually increases at smaller times, therefore, in the present case, all results are presented with a conservative value of $N = 50$. It is found that the increase in computational cost between $N = 10$ and $N = 50$ is not significant, and, therefore, $N = 50$ is a reasonable choice.

Typical transient temperature distribution

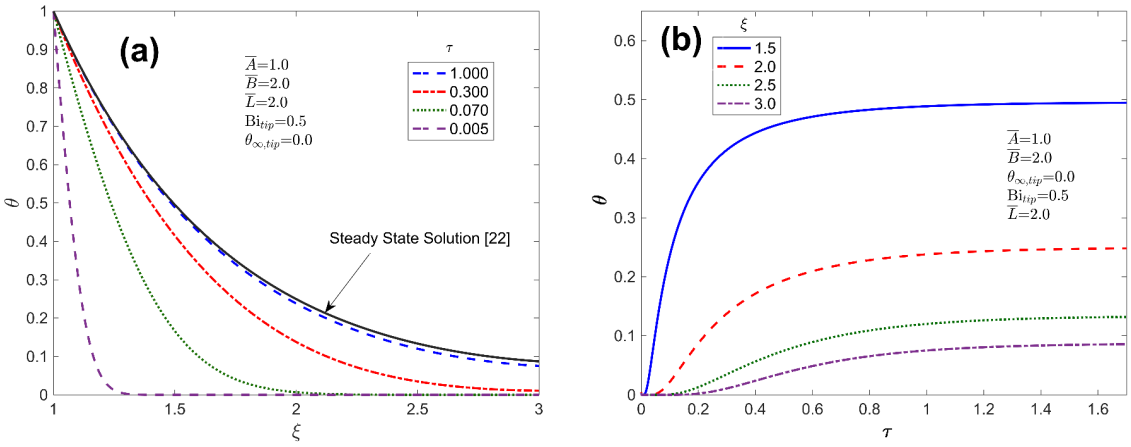

Figure 15. Typical fin temperature field: (a) Fin temperature distribution along the fin at multiple times. (b) Fin temperature at multiple locations as functions of time. The steady state solution is also shown in (a) for reference.

For a fixed set of problem parameters $\bar{A} = 1.0$, $\bar{B} = 2.0, \bar{L} = 2.0$, $Bi_{tip} = 0.5$, $\theta_{tip,\infty} = 0.0$, Figure 15(a) plots temperature distributions in the fin at different times. This is supplemented by plots of temperatures at different fin locations as functions of time in Figure 15(b). Figure 15(a)

shows that thermal transport into the fin causes temperature rise over time, first in regions next to the fin base and slowly encompassing the entire fin. As time passes, a balance is reached between advective/conductive thermal transport into the fin and convective heat removal into the ambient, resulting in steady state. For example, at $\tau = 0.005$, only the region up to $\xi = 1.30$ has heated up significantly, while the rest of the fin is still nearly at the initial temperature. As time passes, the temperature curve shifts rightwards and upwards, indicating deeper and deeper penetration of heat into the fin. At large times, the transient temperature field computed using the model presented here approaches the independently computed steady state profile [22], also shown in Figure 15(a).

It is notable that as time passes, there is a reduction in the slope of the temperature curve at the fin base, which represents the conductive rate of heat removal, per equation (24), indicating reduction in conductive heat removal over time. Temperature curves as functions of time presented in Figure 15(b) show that, depending on how far a point is from the fin base, there is an initial period of negligible temperature rise before temperature begins to rise appreciably. This is mainly due to the time taken for thermal transport from its base to a given fin location. As expected, the closer a point is to the fin base, the shorter is this initial period, the earlier is steady state reached, and, finally, the greater is the temperature rise at steady state.

Impact of advective ($\bar{A}$) and convective ($\bar{B}$) thermal transport

The two key transport-related non-dimensional parameters that appear in the transient porous fin problem are $\bar{A}$ and $\bar{B}$, which represent advective thermal transport down the fin and convective heat removal from the fin, respectively, both expressed relative to the rate of conduction heat

transfer down the fin. The impact of $\bar{A}$ and $\bar{B}$ on the transient temperature field in the fin is examined first, with particular interest in the time taken to reach steady state.

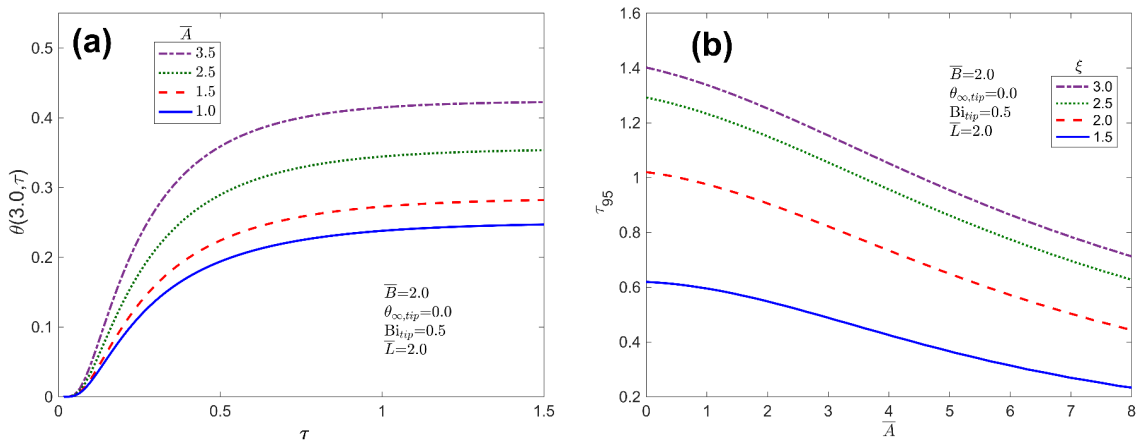

Figure 16. Effect of $\bar{A}$: (a) Fin temperature at tip as a function of time for multiple values of $\bar{A}$, (b) Time required for 95% of temperature change up to steady state as a function of $\bar{A}$ at multiple fin locations.

The transient fin temperature distribution is computed using equations (14) and (22) for several values of $\bar{A}$. All other parameters are held constant as follows: $\bar{B} = 2.0$, $\bar{L} = 2.0$, $Bi_{tip} = 0.5$, $\theta_{\infty,tip} = 0.0$. Since steady state is reached only asymptotically at infinite time, therefore, the time taken for the temperature to reach 95% of the eventual temperature at very large time, denoted by τ_{95} is taken to represent the time to reach steady state. Results are plotted in Figure 16, where Figure 16(a) plots the tip temperature as a function of time for each case and Figure 16(b) plots τ_{95} as a function of $\bar{A}$ at multiple locations on the fin. Several key features of the transient temperature distribution in this problem are evident from Figures 16(a) and 16(b). First of all, there is a small initial time during which there is no significant temperature at the fin tip. This is because of the finite time taken for thermal energy to reach the fin tip due to advection and conduction from the hot base. Following this initial period, temperature rises rapidly, and then

slows down as the fin approaches steady state. Figure 16(a) shows greater temperature rise for larger values of $\bar{A}$, which is expected because $\bar{A}$ represents advective transport of heat. Therefore, the larger the value of $\bar{A}$, the more rapidly does the point of interest heat up. In addition to the magnitude of temperature, $\bar{A}$ also influences the speed at which the fin approaches steady state. This is best observed in Figure 16(b), where the time taken to reach steady state, τ_{95} is found to decrease with increasing $\bar{A}$. Finally, Figure 16(b) also shows that different locations at the fin take different times to reach steady state. The closer a point is to the base, the faster it reaches steady state due to rapid thermal transport from the base to the point. Depending on the value of $\bar{A}$, the time to reach steady state at the fin tip may be 40-50% greater than the time to reach steady state at the mid-point of the fin.

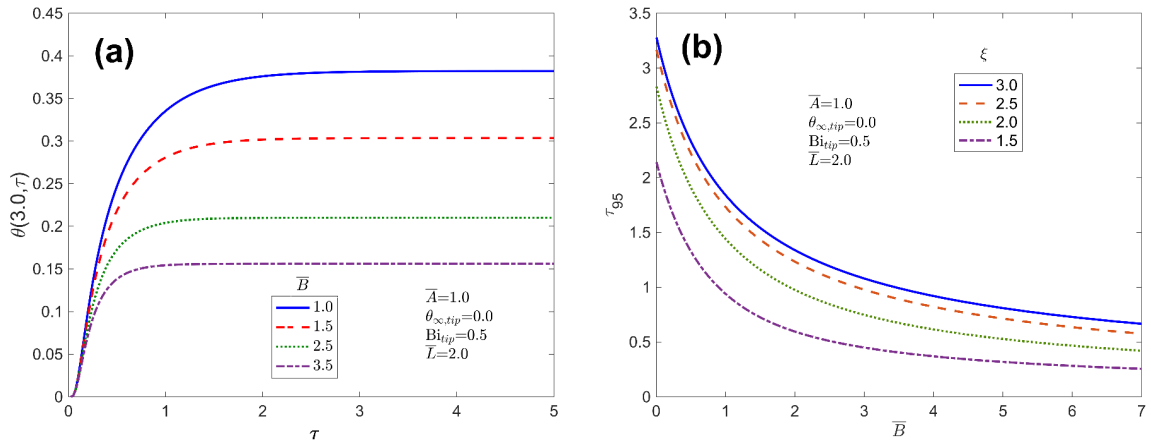

Figure 17. Effect of $\bar{A}$: (a) Fin temperature at tip as a function of time for multiple values of $\bar{A}$, (b) Time required for 95% of temperature change up to steady state as a function of $\bar{A}$ at multiple fin locations.

A similar analysis of the impact of $\bar{B}$ on the transient temperature field is presented in Figure 17. Temperature at the tip of the fin is plotted as a function of time for multiple values of $\bar{B}$ in Figure 17(a), and the time taken to reach steady state is plotted as a function of $\bar{B}$ for multiple locations

on the fin in Figure 17(b). A few aspects of the effect of $\bar{B}$ on the transient temperature field are similar to the effect of $\bar{A}$ – there is an initial period of slow temperature rise, followed by prolonged, rapid temperature rise, eventually leading asymptotically to steady state. Unlike $\bar{A}$, the larger the value of $\bar{B}$, the lower is the temperature rise. This is because $\bar{B}$ represents the rate at which the fin convectively loses heat to the surrounding medium. A larger value of $\bar{B}$ implies greater heat loss, and, therefore, lower temperature. It is found that $\bar{B}$ also has a significant impact on the time taken to reach steady state. At any given location, a large value of $\bar{B}$ results in faster arrival of steady state. This is because large $\bar{B}$ implies greater convective heat removal that counteracts the conductive/advective heat flow from the fin base, resulting in reaching steady state faster.

Heat removal rates as functions of time

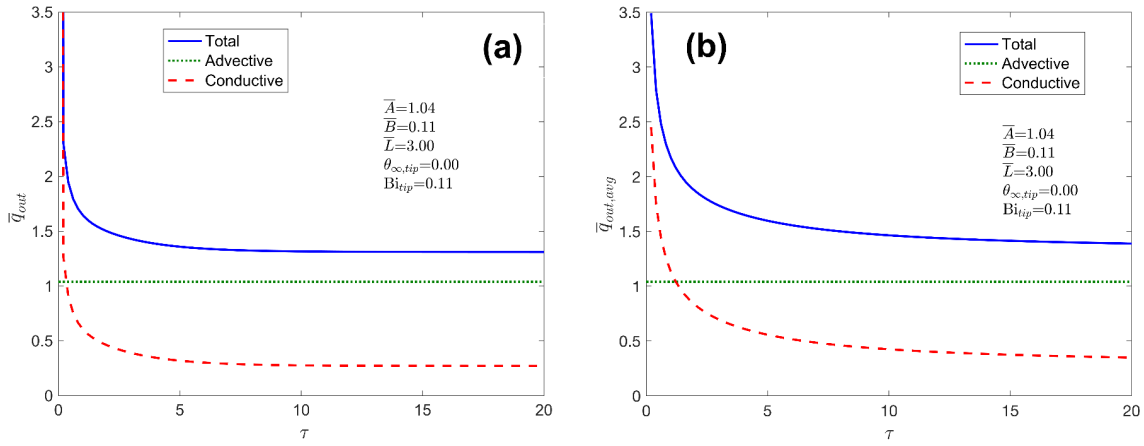

Figure 18. Advective, conductive and total heat removal rates through the fin as functions of time: (a) and (b) present instantaneous and averaged heat removal rates.

The previous sub-section focuses mainly on fin temperature distribution and the time taken to reach steady state. In addition, it is also of much interest to examine how the rate of heat removal by the fin varies with time. While steady state heat removal by the porous fin has been

characterized in the past [22], there are several scenarios, as outlined in Section 1, where only a finite amount of time is available for the heat removal process, during which, the fin may not even reach steady state. In such scenarios, steady state performance of the porous fin is not relevant, and, instead, it is important to understand how heat removal by the fin changes with time prior to reaching steady state. For a fixed set of problem parameters ($\bar{A} = 1.04$, $\bar{B} = 0.11$, $\bar{L} = 3.0$, $Bi_{tip} = 0.11$, $\theta_{\infty,tip} = 0.0$), Figure 18 plots the non-dimensional fin heat removal rate as a function of time. In order to facilitate a fundamental understanding of this problem, both advective and conductive rates of heat removal, as defined by equation (24) are also plotted, in addition to the total heat removal rate. Figure 18(a) plots the instantaneous rates of heat removal, per equation (24), whereas the average rate of heat removal up to a certain time, which may be of greater practical importance, is plotted as a function of time in Figure 18(b). Since the advective rate of heat removal is simply equal to $\bar{A}$, per equation (24), therefore, the advective curves in Figures 6(a) and 6(b) are both horizontal straight lines, corresponding to the value of $\bar{A} = 1.04$ used here. In contrast, the conductive rate of heat removal depends strongly on time. At early times, when there is a large temperature gradient between the fin base and the rest of the fin, there is very large conductive heat removal, per equation (24). As the fin heats up, this temperature difference reduces, and the conductive rate of heat removal drops sharply, eventually reaching a steady value. Trends similar to the instantaneous heat removal rates shown in Figure 18(a) are also found in the average heat removal rates plotted in Figure 18(b). The reduction in conductive rate of heat removal over time seen in Figures 18(a) and 18(b) are consistent with Figure 15(a), where the slope of the temperature field at the fin base, $\left(\frac{\partial\theta}{\partial\xi}\right)_{\xi=1}$ is found to reduce and reach a steady value as time increases.

The plots in Figure 6 show that heat removal at early times is dominated by the conductive mechanism, whereas, there is a certain time at which the two mechanisms have equal contributions (around $\tau = 1.2$, as shown in Figure 18(b)), and at later times, advective heat removal dominates. This shifting away of the dominating mechanism from conductive to advective over time is an important consideration in the design of practical systems when there is only finite time available for heat removal. In such cases, the time available for heat removal must be compared against the transition time shown in Figure 18, based on which, one must design to either enhance advective or conductive heat removal mechanism by changing underlying parameters such as the porosity of the fin or the applied pressure difference. For example, if the total time available is relatively small, then one must maximize conductive heat transport by choosing a low value of porosity, or not using a porous fin at all. In contrast, if the time available for heat transfer is much larger than the conduction-to-advection transition time, then it may be beneficial to improve advective heat removal by increasing fin porosity.

Effect of porosity on fin performance

Porosity is a key parameter in the design of the porous fin. The porosity of the fin material can be easily varied, and must be carefully chosen in order to maximize the desired objective, in most cases, the total heat removed by the fin. Introducing porosity into the fin may impact advective and conductive heat removal mechanisms in opposite directions. For example, greater porosity facilitates greater advective heat removal through increased porous flow down the fin. Mathematically, this occurs due to greater advective component of heat removal given by equation (24), with increasing ϕ. On the other hand, increasing the fin porosity reduces effective thermal conductivity, which reduces conductive heat removal. Due to these opposing effects, it is

of interest to determine if the total heat removed increases or decreases with increasing porosity, or, if there is an optimal value of the porosity that maximizes total heat removed. Past analysis showed that, in steady state, an optimal value of the fin porosity exists under certain conditions, whereas under other conditions, making the fin porous may not be beneficial at all. It is of interest to extend such analysis to transient conditions, in order to facilitate the design of porous fins for scenarios with limited time available for heat transfer.

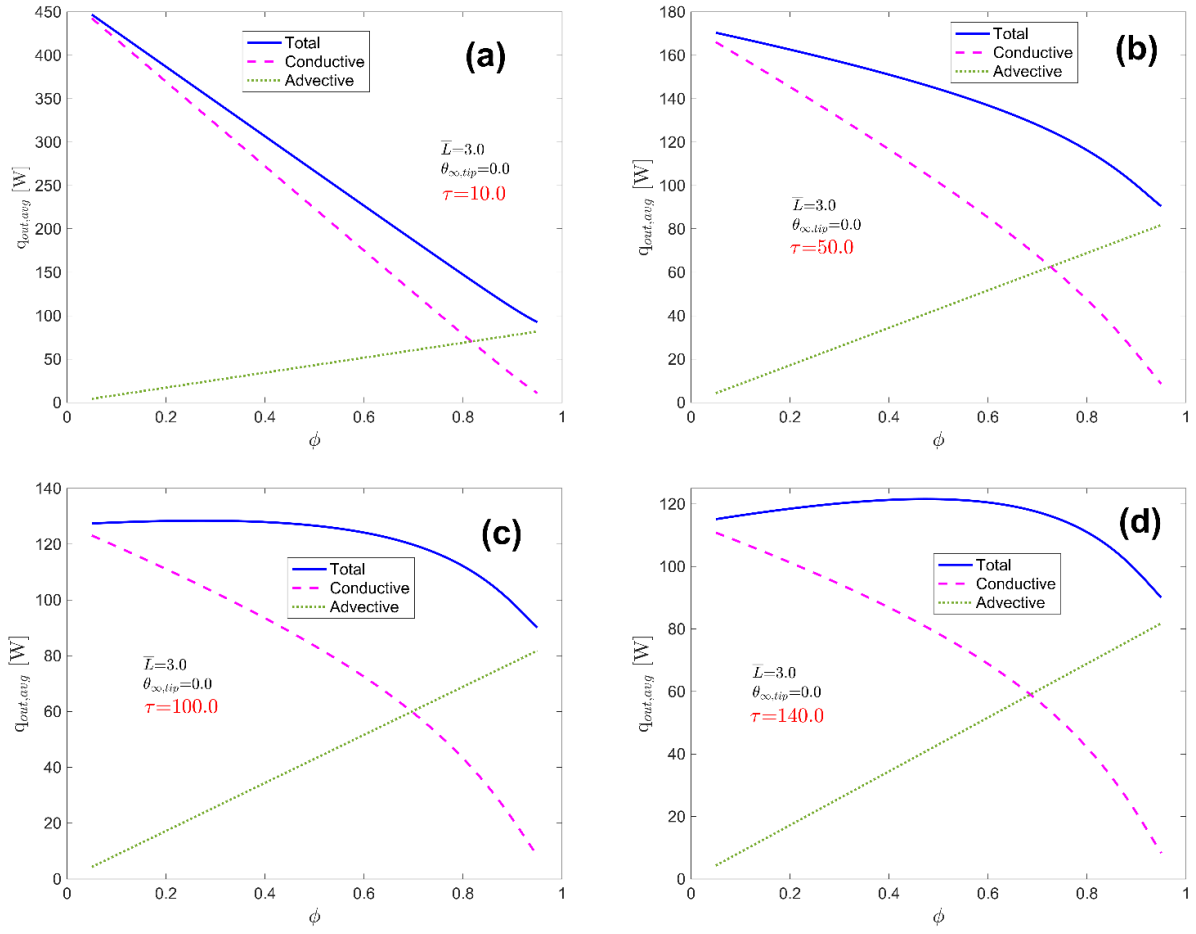

Figure 19. Impact of porosity: Averaged heat removal rates as well as conductive and advective components as functions of porosity up to (a) τ=10.0, (b) τ=50.0, (c) τ=100.0 and (a) τ=140.0.

In order to analyze this problem over a transient time period, the total heat removed as well as its conductive and advective components are plotted as functions of fin porosity in Figure 19. Plots

are presented at four different times. Values of parameters are chosen to be consistent with past steady state analysis [22]. In short, baseline solid and fluid materials are taken to be aluminum and air, with constant properties corresponding to room temperature. Additionally, $K = 5.7 \times 10^{-9}$ m^2, $R_0 = 5$ cm, $L = 15$ cm, $w = 5$ cm, $\Delta p = 100$ Pa, $h = 50$ Wm^{-2}K^{-1}. These plots use equations (14), (21) and (23). Results indicate that at early times, heat removal is dominated by conductive thermal transport, which is due to the large temperature gradient in the fin at small times. As time passes and the fin gets hotter, the temperature gradient reduces, and, therefore, the rate of conductive heat removal reduces sharply. In contrast, the rate of advective heat removal remains invariant with time. As a result of this, it is found that at early times, using a fin with large porosity actually reduces total heat removal, as evidenced by the monotonically reducing plot for the total heat removal in Figures 7(a) and 7(b). This occurs because large porosity results in reduced effective thermal conductivity, and thus a reduction in conductive heat removal, which is the dominant heat removal mechanism at small times. As time passes, the total heat removal curve is found to become more and more curved, as seen in Figure 19(c), and eventually become non-monotonic by developing a maxima at a certain value of porosity, as seen in Figure 19(d). This indicates that if the fin operates for a sufficiently long time, there exists an optimal value of the porosity at which the total heat removal is maximized.

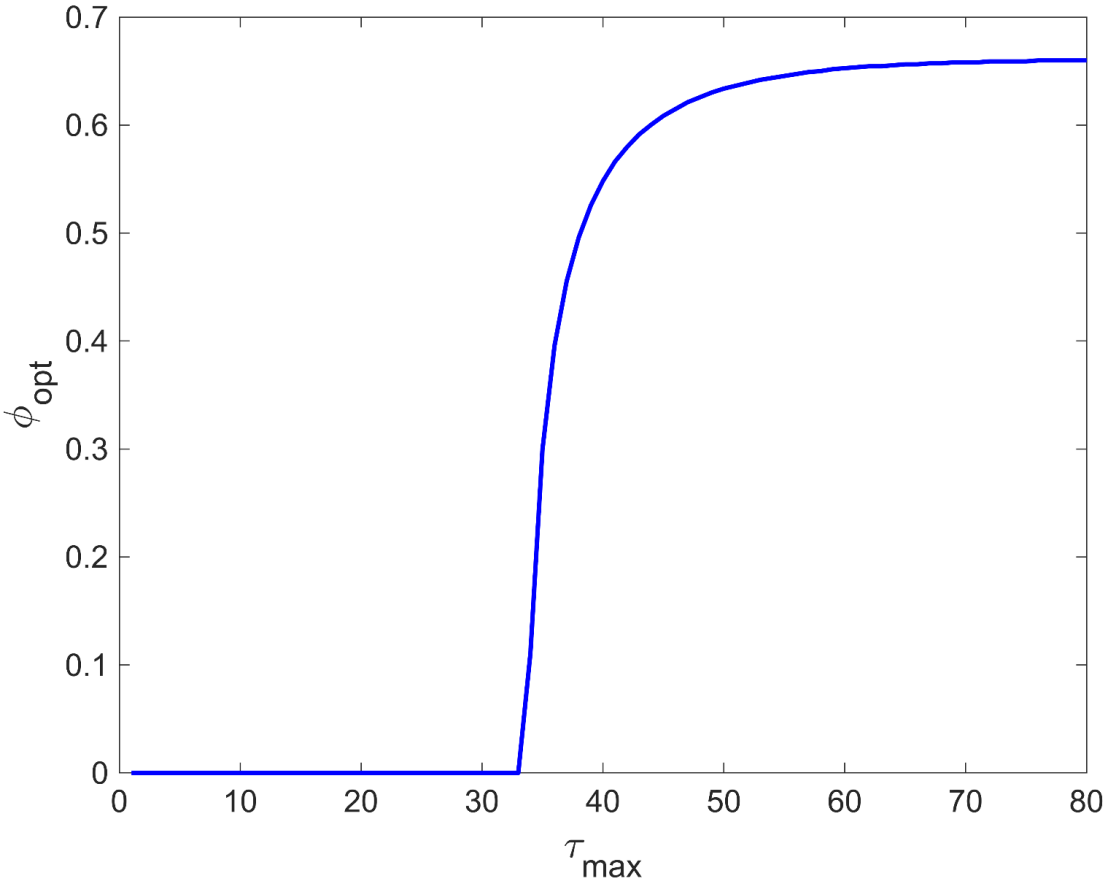

Figure 20. Impact of porosity: Optimal porosity to maximize total heat removal as a function of total time available for heat transfer. Problem parameter are the same as Figure 18.

The optimal porosity of the fin, ϕ_{opt}, is computed and plotted in Figure 20 as a function of the maximum time period available for heat removal, τ_{max} for the same set of parameters as the previous Figure. Figure 20 shows an optimal value of zero porosity for short time periods, due to early dominance of conductive heat removal, which is exacerbated by fin porosity. Beyond a certain time, conductive heat removal has diminished significantly, such that making the fin porous is now favorable. This period in Figure 20 is characterized by a very sharp rise in the value of ϕ_{opt}, followed by saturation at large times, as a steady state is eventually reached, and the optimal value of the fin porosity approaches its value in steady state operation [22]. Note that

porosity values above the optima shown in Figure 20 involve a significant drop in effective thermal conductivity, so as to negate the improvement in advective heat removal. Further, note that the sharpness in the curve shown in Figure 20 is simply because before a certain time period, it is not optimal for the fin to be porous at all, which has been indicated by a zero value for ϕ_{opt} in the curve.

The results presented in this sub-section are of much practical importance in the design of the porous fin for transient heat removal. These results indicate that the choice of how porous the fin is designed to be depends critically, among other factors, on the time period available for heat removal. For short-time heat removal processes, making the fin porous is not helpful at all, as fin porosity worsens thermal conductivity, which directly impacts conductive heat removal that dominates at early times. This loss may not be justified by the additional advective heat removal due to the porous flow when the heat removal time period is short.

Time taken to reach steady state

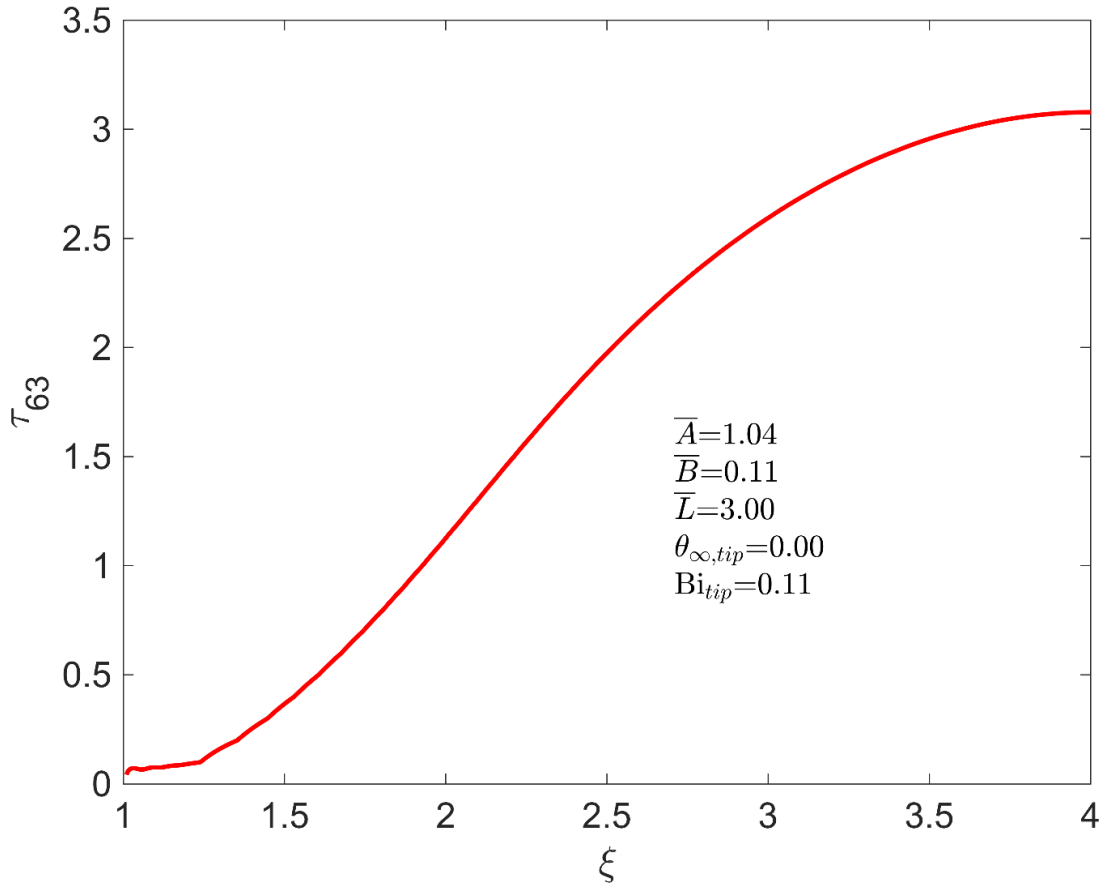

Figure 21. Time required for 63.2% of the temperature change as a function of location along the fin. Parameter values are $\bar{A}$=1.04, $\bar{B}$=0.11, $\bar{L}$=3.0, Bi_{tip}=0.11, $\theta_{\infty,tip}$=0.00.

The time taken to reach steady state is an important performance parameter of interest in transient thermal systems. In the context of a porous fin, this is important to determine in order to ascertain if previously reported steady state characteristics of the porous fin [22] can be used within the time frame of interest. If the operating time of the porous fin is shorter than the characteristic time to steady state, then the transient analysis presented here must be accounted for.

Plots of the total heat removal rate from the fin as a function of time are already presented in Figure 18, from where, the time taken to reach steady state may be estimated. For example, from Figure 18(a), it may be inferred that the instantaneous rate of heat removal reaches within 5% of the eventual steady state value by around $\tau = 5.0$.

A more quantitative representation of time to steady state may be carried out in terms of the transient temperature distribution. Since the initial temperature is known, but the temperature field reaches steady state, in principle, only asymptotically at infinite time, therefore, the time taken to achieve, say, 95% of the temperature change may be used to represent the time taken to reach steady state. Alternately, one may use the classical definition of the thermal time constant of a lumped thermal mass, defined as the time to reach $(1 - 1/e)$, i.e., 63.2% of the temperature change. These quantities are denoted by τ_{95} and τ_{63}, respectively.

Figure 21 plots the time taken to reach 63.2% of the temperature change as a function of spatial location on the fin. Problem parameters are $\bar{A} = 1.0, \bar{B} = 2.0, \bar{L} = 3.0, Bi_{tip} = 0.5, \theta_{\infty,tip} = 0.0$. Note that since the fin is not a lumped thermal mass, therefore, different locations on the fin reach steady state at different rates. Figure 20 shows that fin locations close to the fin base reach steady state very quickly, as expected, due to the physical proximity to the fin base that is responsible for temperature rise. τ_{63} then rises rapidly before reaching a plateau as one approaches the tip of the fin. This is mainly because once far enough from the fin base, the time taken to reach steady state is no longer a strong function of distance from the fin base but instead is influenced more by thermal conditions at the fin tip.

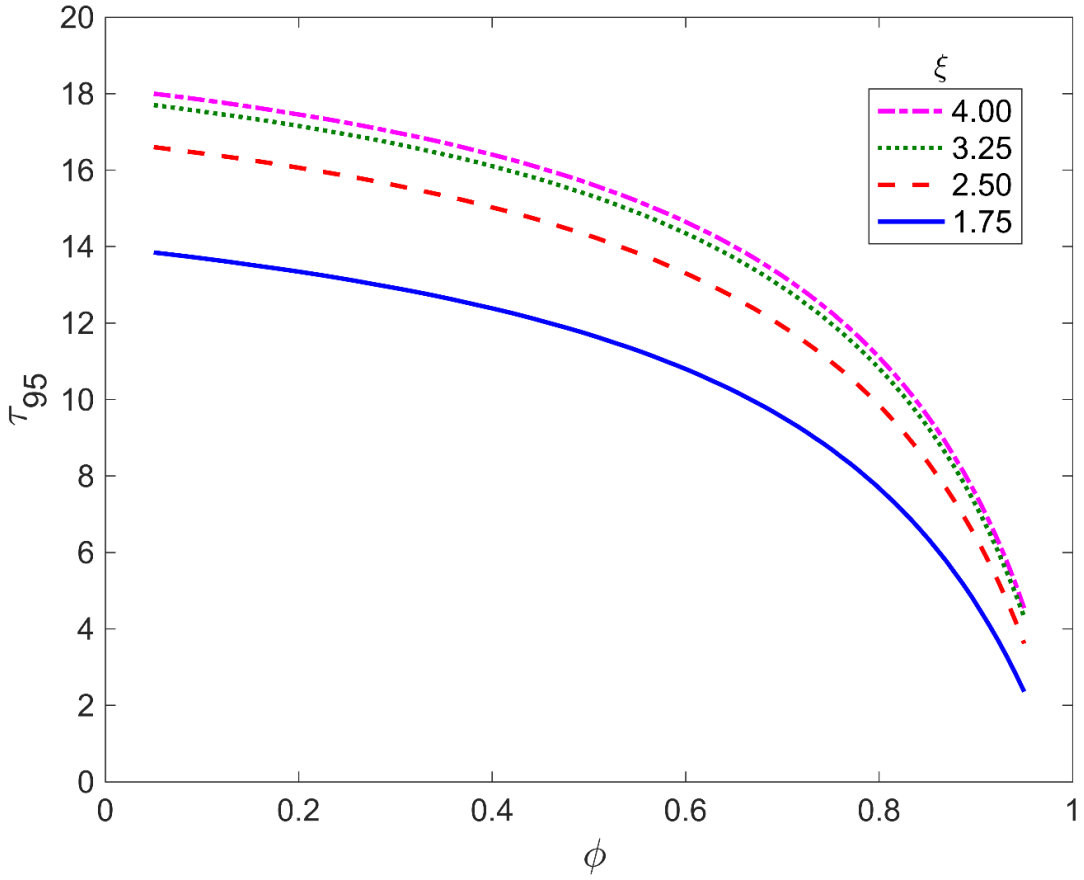

Figure 22. Time required for 95% of the temperature change as a function of porosity at three different fin locations. Parameter values are $\bar{L}$=3.0, $\theta_{\infty,tip}$=0.0.

The time taken to reach steady state is also expected to be a function of fin porosity, because the fin porosity influences the rates of conductive and advective heat removals, which eventually contribute towards reaching steady state. Figure 22 plots τ_{95}, the time taken for 95% of the temperature change as a function of fin porosity. It is found that at each location on the fin, τ_{95} reduces with increasing porosity, slowly at first at small porosities, and more rapidly when the porosity is larger.

Effect of tip conditions

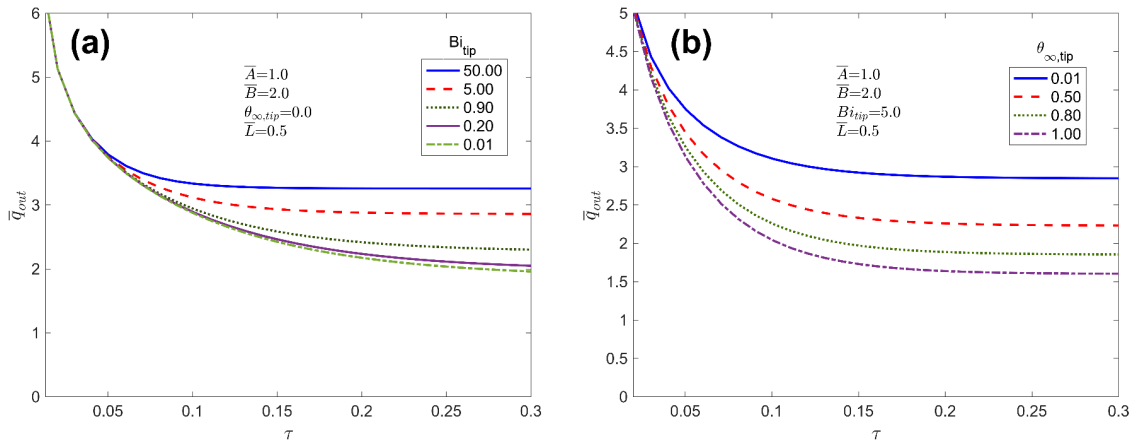

Figure 23. Effect of fin tip conditions: (a) Heat lost through the fin as a function of time for different Bi_{tip}. (b) Heat lost through the fin as a function of time for different $\theta_{\infty,tip}$.

Finally, the effect of fin tip conditions on heat removal rate is examined in Figure 23. The two fin tip parameters of relevance are the fin tip Biot number, Bi_{tip}, representative of the convective heat transfer coefficient at the fin tip, and the fin tip temperature $\theta_{\infty,tip}$. Heat removal rate is plotted as a function of time for different values of these parameters in Figures 23(a) and 23(b), respectively, for a representative set of parameter values. Specifically, the fin length is taken to be $\bar{L} = 0.5$. Figure 23(a) shows that at early times, the heat removal rate does not depend on the Biot number at the tip. This is mainly because at small times, the thermal wave has not reached the tip, and, therefore, the convective heat transfer coefficient at the tip is not yet influential on the heat removal rate. At larger times, the greater the tip Biot number, the greater is the heat removal rate, as expected, due to increased heat removal from the fin tip. In each case, a steady state for the heat removal rate is reached. A large value of Bi_{tip} results in reaching steady state somewhat faster.

Similar to Bi_{tip}, $\theta_{\infty,tip}$ also influences the heat removal rate. Figure 23(b) shows greater heat removal rate for smaller values of $\theta_{\infty,tip}$, as expected, due to the cooling effect at small $\theta_{\infty,tip}$ that induces greater heat removal from the fin base. Similar to Bi_{tip}, heat removal is relatively independent of $\theta_{\infty,tip}$ at small times, and a steady state is reached at large times.

Note that the fin length is expected to play an important role in determining how influential fin tip conditions are on heat removal rate from the fin base. The results presented in Figure 11 are based on a somewhat short fin, $\bar{L} = 0.5$. Calculations for a longer fin, say, $\bar{L} = 2.0$ show that fin tip conditions continue to influence the heat removal rate, but not as strongly as the $\bar{L} = 0.5$ case presented in Figure 23.

Conclusions

The key contribution of the present work is to develop an analytical model for transient performance of a porous fin with radially outwards pressure gradient driven porous flow. Advective heat removal due to such porous flow supplements conductive heat removal. However, the two heat removal mechanisms are influenced differently by key porous properties of the fin, and, therefore, a detailed analysis of transient temperature distribution and the resulting heat removal rate from the fin base is necessary. The analytical solution of the transient CDR equation involving Bessel functions makes it possible to identify important non-dimensional parameters and quantitatively understand their impact on fin performance.

While the steady state performance of such a porous fin has been presented recently, this work addresses the important aspect of transient performance, which may be relevant in a number of practical scenarios, such as battery thermal management, in which, heat removal occurs only for

a short, transient period. In such cases, previously available steady state results are not directly applicable. One interesting result of practical relevance is that the optimal porosity that maximizes heat removal rate depends on the time period over which heat removal by the fin occurs. Such considerations may be important in practical problems that are inherently transient in nature.

References

[1] A.D. Kraus, A.M. Aziz, J.R. Welty, Extended Surface Heat Transfer, John Wiley, New York, 2002.

[2] R.L. Webb, B. Sunden, N.-H. Kim, Principles of Enhanced Heat Transfer, Routledge, Boca Raton, 2005.

[3] D. Harper, W. Brown, 'Mathematical Equations for Heat Conduction in the Fins of Air Cooled Engines,' NACA Report 158, National Advisory Committee on Aeronautics, 1922.

[4] A. Sadeghianjahromi, C.-C. Wang, 'Heat transfer enhancement in fin-and-tube heat exchangers – A review on different mechanisms,' Renewable Sustainable Energy Rev., 137, pp. 110470, 2021. DOI: 10.1016/j.rser.2020.110470

[5] R.J. McGlen, R. Jachuck, S. Lin, 'Integrated thermal management techniques for high power electronic devices,' Appl. Therm. Eng., 24, pp. 1143-1156, 2004. DOI: 10.1016/j.applthermaleng.2003.12.029

[6] A. Mostafavi, M. Parhizi, A. Jain, 'Theoretical modeling and optimization of fin-based enhancement of heat transfer into a phase change material,' Int. J. Heat Mass Transf., 145, pp: 118698:1-10, 2019. DOI: 10.1016/j.ijheatmasstransfer.2019.118698.

[7] T. Ambreen, M.-H. Kim, 'Effect of fin shape on the thermal performance of nanofluid-cooled micro pin-fin heat sinks,' Int. J. Heat Mass Transf., 126, pp. 245-256, 2018. DOI: 10.1016/j.ijheatmasstransfer.2018.05.164

[8] G. Fabbri, ‘Heat transfer optimization in internally finned tubes under laminar flow conditions,’ Int. J. Heat Mass Transf., 41, pp. 1243-1253, 1998. DOI: 10.1016/S0017-9310(97)00209-3

[9] A. Mostafavi, A. Jain, ‘Thermal Management Effectiveness and Efficiency of a Fin Surrounded by a Phase Change Material (PCM),’ Int. J. Heat Mass Transf., 191, pp. 122630, 2022. DOI: 10.1016/j.ijheatmasstransfer.2022.122630

[10] A. Bejan, ‘Entropy generation minimization: The new thermodynamics of finite-size devices and finite-time processes,’ J. Appl. Phys., 79, pp. 1191, 1996. DOI: 10.1063/1.362674

[11] N. Sahiti, F. Krasniqi, Xh. Fejzullahu, J. Bunjaku, A. Muriqi, ‘Entropy generation minimization of a double-pipe pin fin heat exchanger,’ Appl. Therm. Eng., 28, pp. 2337-2344, 2008. DOI: 10.1016/j.applthermaleng.2008.01.026

[12] A. Bejan, M. Almogbel, ‘Constructal T-shaped fins,’ Int. J. Heat Mass Transf., 43, pp. 2101-2115, 2000. DOI: 10.1016/S0017-9310(99)00283-5

[13] M. Turkyilmazoglu, ‘Exact Heat-Transfer Solutions to Radial Fins of General Profile,’ J. Thermophys. Heat Transf., 30, pp. 1-5, 2015. DOI: 10.2514/1.T4555

[14] W. Khan, A. Aziz, ‘Transient heat transfer in a functionally graded convecting longitudinal fin,’ Heat Mass Transf., 48, pp. 1745–1753, 2012. DOI: 10.1007/s00231-012-1020-z

[15] B. Kundu, K.-S. Lee, ‘Analytical tools for calculating the maximum heat transfer of annular stepped fins with internal heat generation and radiation effects,’ Energy, 76, pp. 733-748, 2014. DOI: 10.1016/j.energy.2014.08.071

[16] S. Kiwan, M.A. Al-Nimr, ‘Using Porous Fins for Heat Transfer Enhancement,’ ASME J. Heat Mass Transf., 123, pp. 79-795, 2001. DOI: 10.1115/1.1371922

[17] M. Torabi, H. Yaghoobi, ‘Series solution for convective-radiative porous fin using differential transformation method,’ J. Porous Media, 16, pp. 341–349, 2013. DOI: 10.1615/JPorMedia.v16.i4.60

[18] S.-H. Park, J.H. Jeong, ‘Analytical fin efficiency model for open-cell porous metal fins based on Kelvin cell assumption,’ Int. J. Heat Mass Transf., 196, pp. 123283, 2022. DOI: 10.1016/j.ijheatmasstransfer.2022.123283.

[19] S. Kiwan, ‘Thermal Analysis of Natural Convection Porous Fins,’ Transport in Porous Media, 67, pp. 17-29, 2007. DOI: 10.1007/s11242-006-0010-3

[20] R. Das, ‘Forward and inverse solutions of a conductive, convective and radiative cylindrical porous fin,’ Energy Conv. Management, 87, pp. 96-106, 2014. DOI: 10.1016/j.enconman.2014.06.096

[21] T. Zhao, H. Tian, L. Shi T. Chen, X. Ma, M. Atik, G. Shu, ‘Numerical analysis of flow characteristics and heat transfer of high-temperature exhaust gas through porous fins,’ Appl. Therm. Eng., 165, pp. 114612, 2020. DOI: 10.1016/j.applthermaleng.2019.114612

[22] A. Jain, M. Abbas, M. Torabi, ‘Steady State Thermal Analysis of a Porous Fin with Radially Outwards Fluid Flow,’ Int. J. Heat Mass Transf., 209, pp. 124109:1-12, 2023. DOI: 10.1016/j.ijheatmasstransfer.2023.124109.

[23] J. Mathew, S. Krishnan, ‘A Review on Transient Thermal Management of Electronic Devices,’ J. Electron. Packag., 144, pp. 010801, 2022. DOI: 10.1115/1.4050002

[24] M. Kaviany, Principles of Heat Transfer in Porous Media, 2nd Ed., Springer New York, NY, 1995. DOI: 10.1007/978-1-4612-4254-3

[25] A. Jain, S. McGinty, G. Pontrelli, L. Zhou, ‘Theoretical Modeling of Endovascular Drug Delivery into a Multilayer Arterial Wall from a Drug-Coated Balloon,’ Int. J. Heat Mass Transf., 187, pp. 122572:1-17, 2022. DOI: 10.1016/j.ijheatmasstransfer.2022.122572

[26] E.B. Nauman, Chemical Reaction Design, Optimization and Scaleup, 2nd Ed., John, Wiley & Sons, Hoboken, NJ, 2008 ISBN: 9780470282069

[27] E. Augeraud-Véron, C. Choquet, É. Comte, ‘Optimal Control for a Groundwater Pollution Ruled by a Convection–Diffusion–Reaction Problem,’ J. Optimiz. Theory & Appl., 173, pp. 941–966, 2017. DOI: 10.1007/s10957-016-1017-8

[28] M. Abramowitz, I. Stegun, ‘Handbook of Mathematical Functions,’ United States Department of Commerce National Bureau of Standards, 1964.

[29] A. Jain, M. Parhizi, L. Zhou, ‘Multilayer One-Dimensional Convection-Diffusion-Reaction (CDR) Problem: Analytical Solution and Imaginary Eigenvalue Analysis,’ Int. J. Heat Mass Transfer, 177, pp. 121465:1-11, 2021. DOI: 10.1016/j.ijheatmasstransfer.2021.121465.

APPENDIX A

Derivation of radial velocity field in the porous fin

This Appendix derives an expression for the velocity field in the porous fin. Based on the assumptions listed in Section 2, fluid flow in the fin is driven by the pressure gradient between the inner pipe and the ambient at the fin tip, and is purely radial in nature. Assuming that the porous fluid flow is purely Darcian in nature, the following relationship exists between the volumetric flow rate q and local pressure gradient at any location r:

$$q = \frac{\mathrm{K}A}{\mu}\frac{dp}{dr} \tag{A.1}$$

Where $A = 2\pi rh(1-\phi)$ is the cross-section area for fluid flow at the radial location r, and K, ϕ, and μ are the permeability, porosity and viscosity, respectively. Rearranging and integrating equation (A.1) between $r = R_0$ and $r = R_0 + L$ results in

$$q = \frac{\mathrm{K}A}{\mu \cdot \ln\left(\frac{R_0 + L}{R_0}\right)}\frac{\Delta p}{r} \tag{A.2}$$

Where Δp is the total pressure difference between the inner tube and the fin tip. Finally, since $q = A \cdot U(r)$, therefore, the following expression for the velocity field may be written:

$$U(r) = \frac{\mathrm{K}}{\mu \cdot \ln\left(\frac{R_0 + L}{R_0}\right)}\frac{\Delta p}{r} \tag{2}$$

This completes the derivation of the radial velocity field in the porous fin. As expected, the radial velocity has a $1/r$ dependence, due to the requirement of mass conservation as the fluid flows radially outwards.